npj | science of food

Article

Published in partnership with Beijing Technology and Business University & International Union of Food Science and Technology

https://doi.org/10.1038/s41538-026-00710-0

# Fabrication of stabilized pickering emulsions via crosslinking modified soy protein: focused on fat substitution strategies



Yilin Sun[1], Wenqian Guo[1], Xuejian Li[1], Ling Guo[1,2,3], Yujun Jiang[1,2,3] & Yu Zhang[1,2] ✉

In this study, soy protein isolate (SPI) was modified by ultrasound combined with laccase, and whey protein (WPI) was introduced to stabilize Pickering emulsions by the interaction between composite protein particles. The results indicated that WPI enhanced the stability of modified SPI nanoparticles through hydrophobic interactions and disulfide bond interactions. The adsorption characteristics of the composite nanoparticles at the oil–water interface were assessed by using a real-time quartz crystal microbalance (QCM). The SPI treated with 300 W ultrasonic-enzyme and cross-linked WPI sample (SW3) has the best apparent viscosity, and can rapidly adsorb and form a film layer at the oil–water interface. The SW3 stable emulsion has a relatively high stirring foaming rate (38.24%) in low-fat cream processing, improving the structural stability of 3D printed products. The findings could provide interesting research significance for the application of 3D printed functional foods and Pickering emulsions in food.

Pickering emulsions are stabilized by the irreversible adsorption of natural colloidal particles at the oil–water interface[1]. Various food-grade particles such as carbohydrate polymers, different proteins, and protein–polysaccharide complexes are developed as suitable biopolymer surfactants for Pickering emulsions stabilization[2]. Protein-based colloidal particles have proven to be excellent Pickering emulsifier stabilizers. They can provide satisfactory interfacial activity and interact with the oil phase to stabilize emulsions[3]. Soy protein isolate (SPI) is an amphiphilic protein and has been widely studied as an excellent source of alternative animal protein. The limited interfacial adsorption capacity of natural SPI particles and their instability under high oil phase or complex processing conditions limit their application in functional foods. Appropriate ultrasonic treatment can open the structure of protein, expose more enzymatic catalytic sites, and make the spatial structure more stable[4]. Studies have revealed that stabilizing Pickering emulsions by complexing proteins with other natural macromolecules to form composite nanoparticles can exhibit better emulsifier performance than proteins alone. Türker. (2025) investigated the synergistic effect of zein and charged polysaccharide, and the results revealed that it can significantly improve the stability of Pickering emulsions[5]. Jiang et al. (2025) evaluated the effect of interfacial rigidity on the rheological properties of emulsions prepared from the composite of walnut protein isolate and casein[6]. Whey protein isolate (WPI) has high nutritional value, excellent emulsification and high bioavailability, making it widely used in nutritional health products and infant formula[7]. Thus, the aim of this study is to combine the modified SPI with WPI nanoparticles to develop Pickering emulsions with higher stability and assess their application in the food processing system.

Currently, the increasing demand of consumers for low-fat and high-nutrition foods is. The fresh cream system is complex and unstable, and its high fat content poses potential health risks to consumers[8]. Therefore, the concept of low-fat cream has gradually developed into a strategy. Compared with fat (9 kcal/g), protein has a lower energy density (4 kcal/g) and good foaming ability, and is usually used as a fat substitute[9]. By constructing protein complex particles to stabilize the Pickering emulsions and replace part of the fat in traditional cream, the fat content is reduced while maintaining a similar texture. The development of 3D printing inks that have both health performance and functional adaptability has become a research hotspot. The traditional emulsion inks currently used for extrusion 3D printing rely on inorganic and synthetic particles as emulsifiers, which makes it difficult to meet the requirements of 3D printing for material rheological properties[10]. Pickering emulsions are considered ideal for 3D printing inks with satisfactory stability and flow behavior under extrusion. Due to its unique solid-like characteristics, it can effectively replace part of

[1]Key Laboratory of Dairy Science, Ministry of Education, Department of Food Science, Northeast Agricultural University, Harbin, China. [2]Key Laboratory of Infant Formula Food, State Administration for Market Regulation, Harbin, China. [3]Food Laboratory of Zhongyuan, Luohe, Henan, China. ✉e-mail: jessedevil@163.com

the fat of high-fat foods such as cream and salad dressing, and reduce the fat intake of consumers. Shahbazi et al. (2021) prepared a low-fat soy-based emulsion gel and printed it as an ink into low-fat plant-based meat with good 3D printing performance and quality[11]. A previous study revealed that combining egg yolk granules with chitosan to construct a low-fat Pickering emulsion gel makes it an effective alternative to mayonnaise[12]. Therefore, it is of great significance to construct a Pickering emulsion stabilized by composite dual-protein nanoparticles as a printable ink for 3D printing and apply it to fat substitutes and texture improvers in food production.

Mixed two-protein systems have been reported to have a positive effect on the stability of stable emulsions, especially when proteins with different structural characteristics are used[1,6]. No studies have yet been conducted based on fat substitution strategies to apply the dual-protein emulsion system in improving the foam stability and whipping rate of low-fat whipping cream. Recently, the dissipative quartz crystal microbalance (QCM-D), as a sensitive real-time measurement technology, can reflect detailed characterization information (such as adsorption/desorption properties, adsorption mass, viscoelasticity, etc.), and has high value for the application of molecular interface behavior[13]. Therefore, in this study, soybean protein isolate was modified by ultrasound combined with enzyme crosslinking, and then the two-protein composite nanoparticle stabilized Pickering emulsions were constructed in collaboration with WPI. The interfacial adsorption and rheological properties of Pickering emulsions stabilized by composite nanoparticles were investigated using a QCM-D rheometer. Impressively, we applied it to a low-fat cream system, studying its quality properties and 3D printing capabilities (Fig. 1). This study can provide valuable insights into the use of Pickering emulsions stabilized by two-protein composite nanoparticles as edible 3D printing inks.

## Results

### Selection of the SPI/WPI compounding ratio

In this study, different ratios (5:0, 3:1, 1:1, 1:3, 0:5) of SPI–WPI composite protein particles were prepared and evaluated based on their average particle size, Zeta potential, and microstructure. The results exhibited in Fig. S1A indicated that compared with the single SPI (326 nm), as the quality ratio of SPI:WPI in the composite decreased from 3:1 to 1:1, the average particle size of the composite SPI/WPI particles gradually decreased. At SPI–WPI (1:1), it reached 168 nm, and the polydispersity index (PDI) dropped to 0.12, indicating the formation of homogeneous nanoparticles. As shown in Fig. S1B, both WPI and SPI have weak negative Zeta potential (<20 mV), which results in a lower surface charge on the microstructure and partially explains the self-aggregation. The negative charge of the double protein nanoparticles after the composite was formed was much higher than that of the single SPI (27 mV), especially at the 1:1 ratio, with the absolute value of the charge reaching a maximum of 38 mV. This indicated that at this ratio, the proteins were more unfolded and exposed more charged groups, making them more stable. The SEM results (S1C) revealed that at SPI–WPI (1:1), the microstructure was denser, which is consistent with the results of the average particle size. Therefore, when the SPI:WPI ratio was 1:1, this composite had the largest Zeta potential absolute value and the smallest average particle size, showing the lowest surface hydrophobicity. This is consistent with the research results of Han et al. (2022) and Cui et al. (2024)[14,15]. This ratio was applied in subsequent experiments of modified nanoparticles and Pickering emulsions.

### Characterization and interaction of MSPI/WPI composite nanoparticle

UV absorption spectroscopy can be used as an effective method to reflect the interaction between protein structures and other substances. The characteristic absorption peaks of conjugated double bonds of tryptophan and tyrosine residues are located at 280 nm[16]. As depicted in Fig. 2A, the maximum absorption bands of SPI occurred at 202 and 270 nm. The change in the position or height of the characteristic peak of the UV spectrum indicates that the microenvironment of aromatic amino acid residues in the protein molecule has changed, resulting in a change in the protein conformation[17]. The maximum absorption peaks of the composite nanoparticles (SW1–SW5) have redshifted compared with a single SPI, indicating that the intermolecular interactions between proteins expose more amino acid residues within the molecules to the surrounding solvents (Fig. 2A). Xie et al. (2025) studied the ultraviolet spectral absorption of the complex of corn protein and ovalbumin and obtained similar results[18].

Fluorescence spectroscopy has been widely used to monitor the changes in the tertiary structure of proteins interacting with other molecules[19]. As shown in Fig. 2B, when the excitation wavelength was

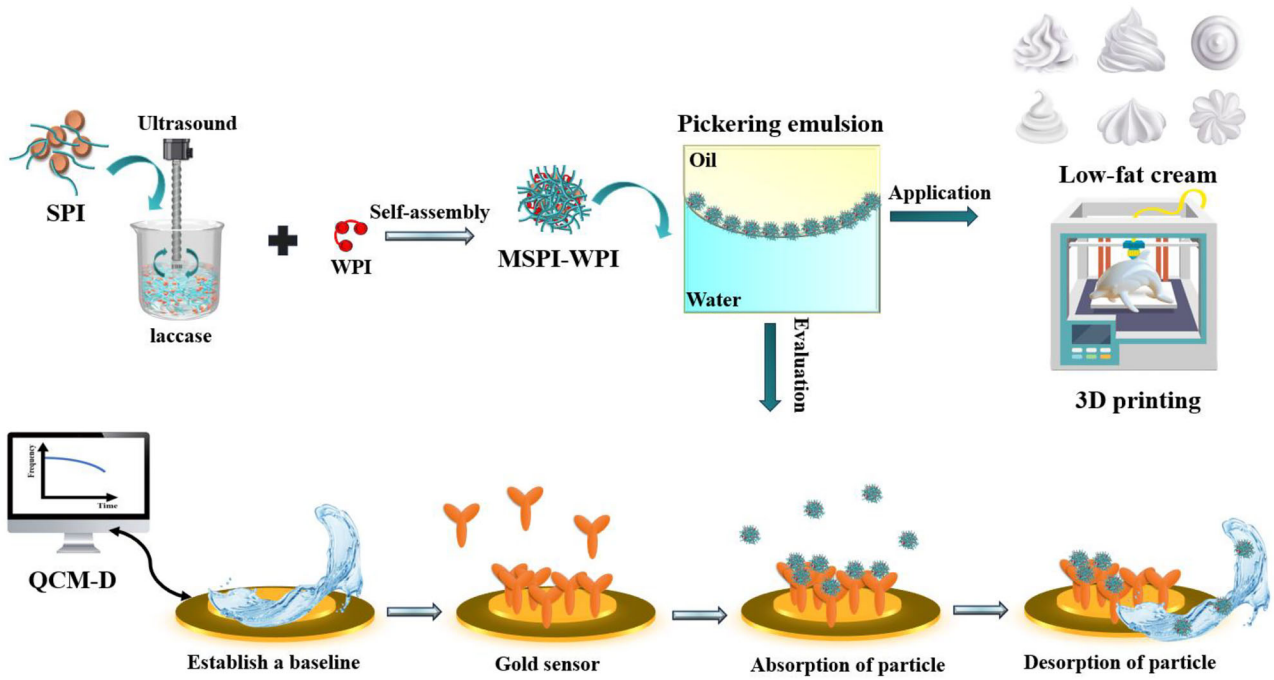


**Fig. 1 | Schematic diagram of the synthesis, application of MSPI–WPI composite nanoparticles, and their adsorption and desorption behaviors at the oil–water interface of Pickering emulsion.** MSPI modified soy protein isolate, WPI whey protein, QCM-D quartz crystal microbalance with dissipation.

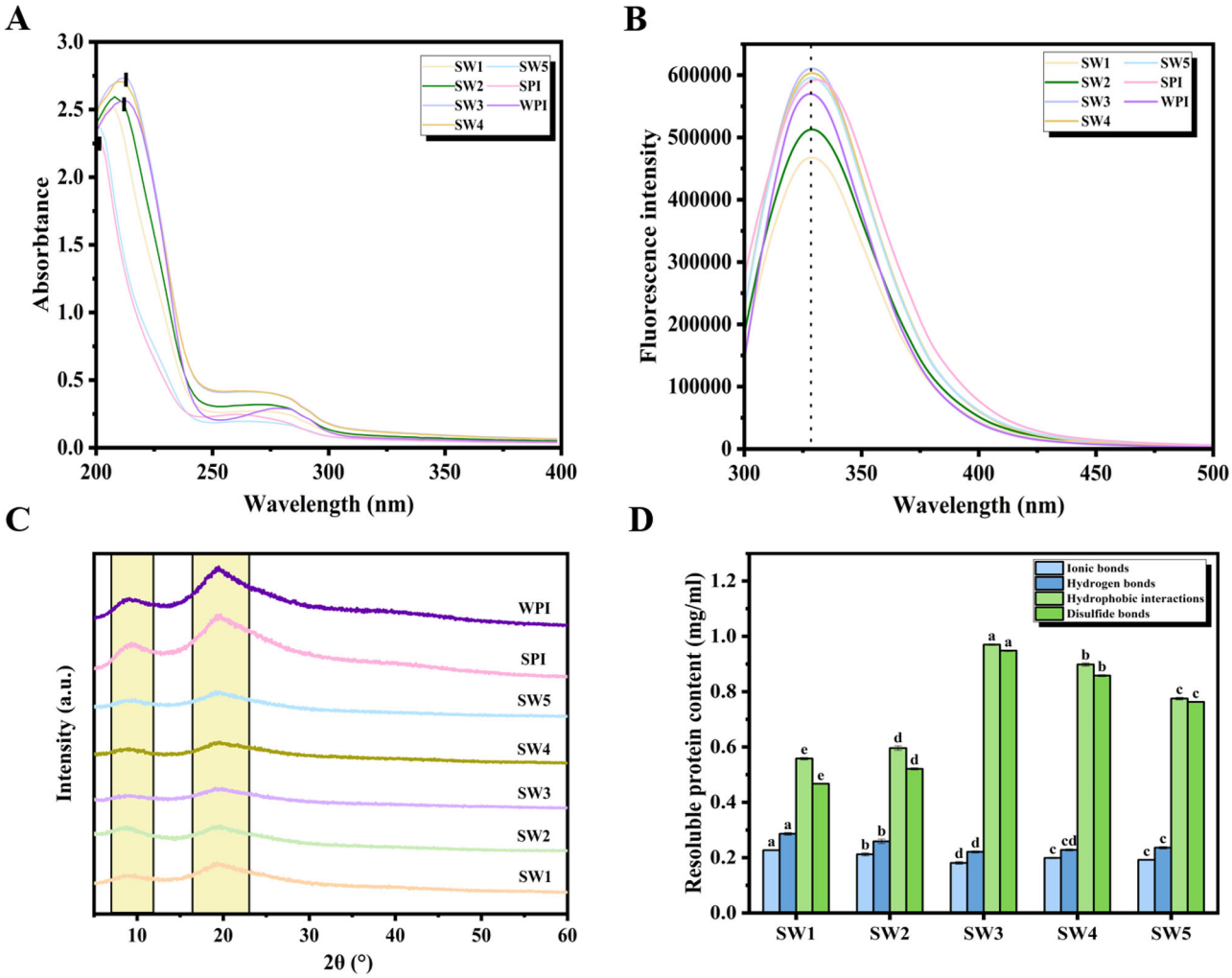


**Fig. 2 | Structural characterization and interaction analysis of composite protein nanoparticles.** UV absorption spectra analysis (**A**), fluorescence spectroscopy analysis (**B**), XRD profiles (**C**), and intermolecular forces (**D**). All the values are expressed as mean ± SD. Mean values with different letters are significantly different ($p < 0.05$). SW1: Ultrasonic (0 W)—laccase-modified SPI cross-linked WPI; SW2: Ultrasonic (150 W)—laccase-modified SPI cross-linked WPI; SW3: Ultrasonic (300 W)—laccase-modified SPI cross-linked WPI; SW4: Ultrasonic (450 W)—laccase-modified SPI cross-linked WPI; SW5: Ultrasonic (600 W)—laccase-modified SPI cross-linked WPI; SPI soy protein isolate, WPI whey protein.

280 nm, the maximum absorption peak of the SPI sample was at 340 nm, which is consistent with the previous results[20]. The maximum emission wavelength of the composite nanoparticles (SW1–SW2) occurs at 330 nm, and the fluorescence intensity was decreased compared with the SPI sample. However, the fluorescence intensity of the composite nanoparticles (SW3–SW5) has increased. This is because high-intensity ultrasound opens up the structure of the complex protein, releasing the previously concealed Trp residues from the binding interfaces between the complex proteins, while exposing more hydrophobic groups to the protein molecules[21]. Jin et al. (2024) also found that the intensity of the fluorescence emission peak increased after the combination of pea isolate protein and whey isolate protein[22].

XRD is an effective method for studying crystal transitions[23]. As illustrated in Fig. 2C, SPI and WPI present two wide peaks near $2\theta = 9.6°$ and 19.5°, respectively. In the XRD patterns of the composite nanoparticles, it was found that the diffraction Angle formed by the crystallization peaks near 19.3° in the crystallization region becomes larger, and the intensity decreases. This indicated that the interaction between MSPI and WPI leads to structural rearrangement, forming new and more disordered complexes, resulting in a reduction in crystal size. Liu et al. (2024) revealed that after being processed by extrusion technology, all the peaks of the composite protein particles weakened, indicating that most of the crystal structure had been destroyed[24]. Therefore, the composite nanoparticles form a greater degree of amorphous structure and lower stiffness[25].

Evaluating the solubility of nanoparticles in different solvents can reveal the types of protein interactions (Fig. 2D). The findings exhibited that hydrophobic interactions and disulfide bonds contribute the most to the formation of composite nanoparticles. This is because ultrasound combined with enzyme cross-linking can lead to protein denaturation and exposure of hydrophobic groups, promoting the formation of disulfide bonds and hydrophobic interactions. Chen et al. (2023) have demonstrated that hydrophobic interactions and disulfide bonds between molecules are the main chemical forces maintaining myosin heat-induced gels[26]. Disulfide bonds are also very important in the formation of protein gels induced by enzyme cross-linking. The increase in disulfide bonds and hydrophobic interactions (SW3) indicated an enhanced degree of cross-linking between protein molecules, which was conducive to the formation of ordered cross-linking networks[26].

Interfacial tension is an effective index to measure the emulsification ability of particles. It can be seen from Fig. 3A that the interfacial tension of the composite nanoparticles at the oil-water interface decreases rapidly with the increase of time, indicating that proteins are gradually adsorbed to the

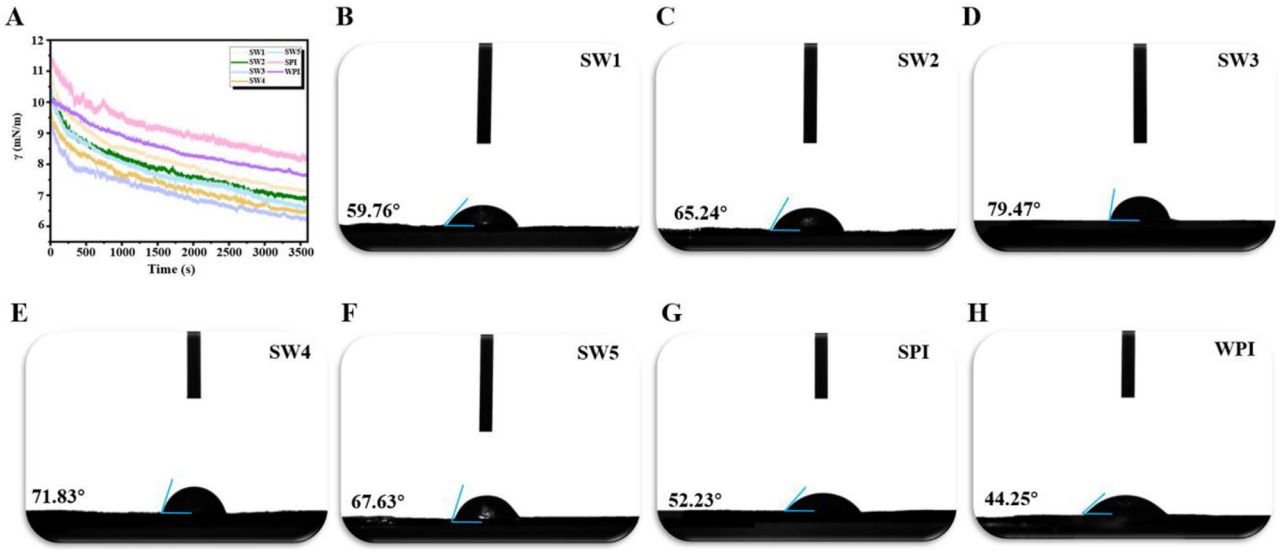


**Fig. 3 | Interfacial interaction analysis of composite protein nanoparticles.** The interfacial tension (**A**) and water contact angle (**B**–**H**) of the solution formed by composite nanoparticles. SW1: Ultrasonic (0 W)—laccase-modified SPI cross-linked WPI, SW2: Ultrasonic (150 W)—laccase-modified SPI cross-linked WPI, SW3: Ultrasonic (300 W)—laccase-modified SPI cross-linked WPI, SW4: Ultrasonic (450 W)—laccase-modified SPI cross-linked WPI, SW5: Ultrasonic (600 W)—laccase-modified SPI cross-linked WPI, SPI soy protein isolate, WPI whey protein.

oil-water interface. Laccase-assisted ultrasonic treatment led to the denaturation and expansion of SPI proteins, exposing more hydrophobic groups in the composite nanoparticles. The interaction with oil droplets promoted the rapid adsorption of proteins[27]. However, with the increase of the number of adsorbed proteins, the number of adsorbed proteins gradually tends to be saturated, and the adsorbed proteins will undergo structural rearrangement at the interface, which hinders the continued adsorption of proteins[28]. The results shown in Fig. 3A indicated that the interfacial tension of the composite particles (SW3) was much lower than that of SPI, which was conducive to the formation of a stable emulsification system. Zhao et al. (2025) exhibited that the overall interfacial tension of soy protein amyloid fiber was lower than that of SPI, indicating that it maximally reduced the interfacial tension between the aqueous phase and the oil phase[29].

Some wettable particles enhance the adsorption, aggregation, and accumulation of colloidal particles at the interface, thus forming a steric barrier to prevent aggregation[6]. The measurement of a three-phase antenna at the air-water interface is helpful to evaluate the hydrophobicity and hydrophilicity of protein nanoparticles. As shown in Fig. 3B–H, the contact angles of SPI and WPI are 55.23° and 44.25°, indicating that the particles are more hydrophilic and more inclined to form oil-in-water (O/W) emulsions[30]. The contact angle of the composite nanoparticles showed a trend of increasing first and then decreasing. Among them, the contact angle of the SW3 group was the largest at 79.47°, close to 90°, which was consistent with the optimal angle at which the emulsifier anchored at the interface, thus promoting the stability of the oil-in-water emulsion.

### The microscopic scale of composite nanoparticles

The particle size and zeta potential of MSPI–WPI composite nanoparticles were characterized (Fig. 4A). Compared with the SPI group, the average particle size of the composite nanoparticles was significantly reduced ($p < 0.05$). This might be because low-frequency ultrasound combined with enzyme cross-linking enhances the interaction between proteins, making them bind more tightly[31]. Li et al. (2021) also found that appropriate ultrasonic power can make protein particles smaller, attributed to the powerful destructive force of ultrasonic waves, which disrupts the electrostatic interactions, hydrogen bonds, and other non-covalent forces between proteins[32]. However, the average particle size of SW5 particles increased, indicating that the aggregation of complex protein particles occurred again. Zeta potential is one of the most used methods to evaluate the surface charge of solid particles and the stability of dispersed systems[33]. As shown in Fig. 4A, the zeta potential of all nanoparticles is negatively charged. The absolute value of the zeta potential >20 mV indicates that the colloidal system is more stable[34]. Compared with a single protein, the absolute value of complex protein potential was larger, especially SW3, which showed a potential of −32 mV ($p < 0.05$). The results revealed that the internal and external charge distribution of the two protein nanoparticles was optimized after the composite treatment, which promoted electrostatic repulsion and enhanced particle stability.

TEM images further confirmed the formation of composite MSPI–WPI nanoparticles (Fig. 4B–H). The complexes without ultrasonic treatment were in an aggregated state. The size of the dual-protein particles constructed by ultrasonically modified MSPI first decreased and then increased (SW2–SW5). This result is consistent with Huang et al. (2020). Huang et al. (2020) also found that ultrasound of different intensities would lead to the reduction and aggregation of protein particle size[35].

### Evaluation of properties of nanoparticle-stabilized Pickering emulsion

The rheological property of the emulsion can be used as a powerful index to detect the complex structure of Pickering emulsions. In the frequency range of 0.1–10 Hz, the energy storage modulus of all emulsions exceeds the loss modulus (Fig. 5A and B). The energy storage modulus and loss modulus of SW3 emulsion are higher than those of other complex protein particle stable emulsions, indicating excellent viscoelasticity. Gao et al. (2023) have shown that when the viscosity and modulus are high, they may restrict the flow of emulsion droplets and hinder phase separation, thus making the emulsion more stable[36]. Moderate ultrasonic treatment changed the structure of SPI, thereby enhancing the bonding strength with WPI, reducing the interfacial tension to a greater extent, and forming a dense interfacial layer structure. However, due to the molecular aggregation of SW5 composite nanoparticles, the interfacial adsorption capacity and viscoelasticity of complex proteins are reduced[37]. As depicted in Fig. 5C, the apparent viscosity of all emulsions decreased with the increase of shear rate, especially the SW3-stabilized emulsions showed shear thinning behavior. It showed that SW3 has the highest stability due to the decrease in droplet migration rate.

The stability of the emulsion was positively correlated with the adsorption amount of interfacial protein[38]. The adsorption capacity of the interface protein in SW1 emulsion was 54.98%, and that of SPI was 52.49%

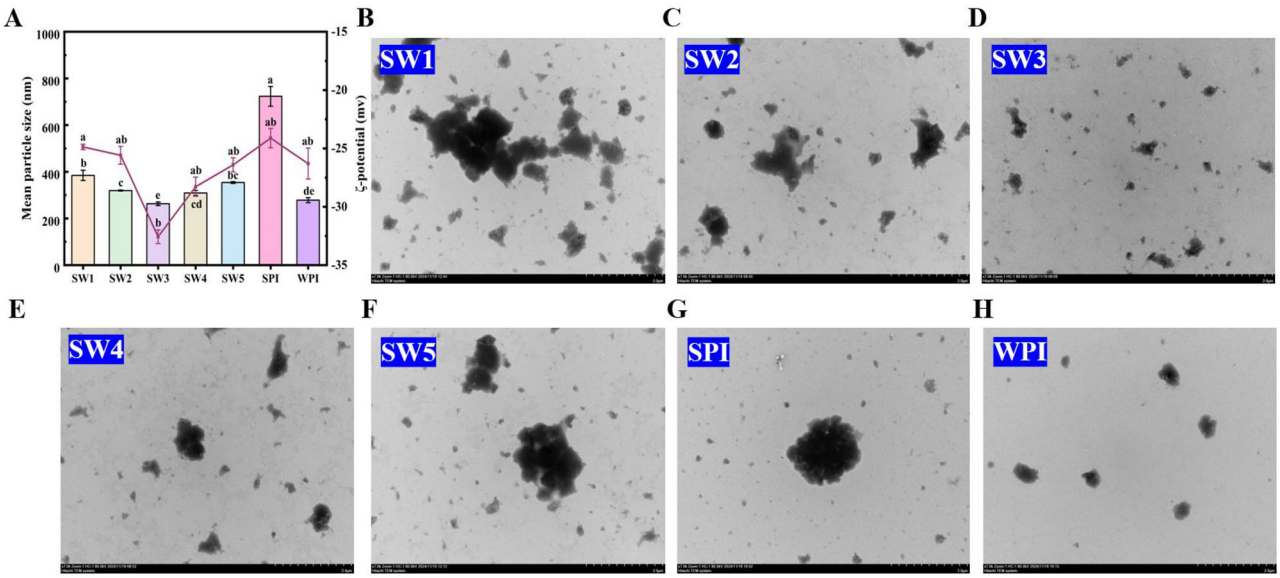


**Fig. 4 | Microlevel analysis of composite protein nanoparticle formation.** Particle size potential (**A**) and transmission electron microscopy (**B**–**H**) of the solution formed by composite nanoparticles. All the values are expressed as mean ± SD. Mean values with different letters are significantly different ($p < 0.05$). SW1: Ultrasonic (0 W)—laccase-modified SPI cross-linked WPI; SW2: Ultrasonic (150 W)—laccase-modified SPI cross-linked WPI; SW3: Ultrasonic (300 W)—laccase-modified SPI cross-linked WPI; SW4: Ultrasonic (450 W)—laccase-modified SPI cross-linked WPI; SW5: Ultrasonic (600 W)—laccase-modified SPI cross-linked WPI. SPI soy protein isolate, WPI whey protein.

(Fig. 5D). Compared with the SPI group, the interfacial protein adsorption content of the emulsion stabilized by composite nanoparticles increased significantly ($p < 0.05$), especially in the SW3 group, where the AP reached the maximum value of 66.12%. This is mainly due to the positive effect of the SW3 group samples on the protein conformation, allowing the complex protein molecular structure to unfold, thereby accelerating the adsorption rate of proteins at the oil–water interface. Ye et al. (2025) also conducted research revealing that ultrasonic treatment can alter the spatial arrangement of protein structures in rapeseed and increase its specific surface area[39].

### Quartz crystal microbalance (QCM)

QCM-D is a highly sensitive surface analysis technique. QCM-D was utilized to investigate the interfacial adsorption and desorption behaviors of composite nanoparticles in the oil–water interface layer of Pickering emulsions. The curves of frequency change $\Delta f$ and dissipation change $\Delta D$ were revealed in Fig. 6A and B, respectively. Negative $\Delta f$ and positive $\Delta D$ displacements were observed, indicating that the composite nanoparticles were deposited on the surface of the sensor[40]. In the sample system of the SW3 group, it can be observed that the changes of this complex at 1500 s (0–1500 s, $\Delta f$ rapidly decreases, $\Delta D$ slightly increases). This phenomenon can be attributed to the rapid adsorption of particles on the hydrophobic surface. When most of the adsorption sites are filled, the emulsifier at the interface reaches a saturated state. Subsequently, the particle complex cross-links and rearranges at the oil–water (O/W) interface (1500s–5500s, $\Delta f$ slowly and continuously decreases, $\Delta D$ continuously increases). This result indicated that the sample deposition speed slowed down, and most of the adsorption sites were occupied by WPI emulsifier[41]. After 5500 s, the composite particles are stable at the O/W interface layer ($\Delta f/\Delta D$ tends to be flat).

Then, the system was rinsed with ultra-pure water (Stage 2) to remove any loosely bound or unabsorbed emulsifiers in the system. This resulted in an increase in $\Delta f$ for all emulsifiers, indicating that some emulsifier molecules had been removed from the surface. The SW3 composite nanoparticles rapidly adsorbed onto the hydrophobic surface. $\Delta D$ is widely used to distinguish soft viscoelastic layers ($>1 \times 10^{-6}$) or rigid viscoelastic layers ($<1 \times 10^{-6}$). As shown in Fig. 6A, the final $\Delta D$ value of the sample after rinsing ($>1 \times 10^{-6}$) indicated that all the adsorbed layers were soft viscoelastic. The increase in $\Delta D$ means that the energy on the quartz crystal was rapidly dissipated, thereby forming a softer sample membrane[42]. Among them, the high energy dissipation ($\Delta D = 3.62 \times 10^{-6}$ Hz) measured by SW3 on the quartz crystal surface can be attributed to the formation of a soft and viscoelastic emulsifier layer. In terms of frequency variation, the $\Delta f$ of SW3 was −37 Hz, whose absolute value is much higher than that of a single SPI (−8 Hz) and WPI (−29 Hz); the $\Delta f$ of other protein particle samples is concentrated around −25 Hz; these results indicate that the SW3 sample shows the highest adsorption and binding affinity to the hydrophobic surface. Therefore, the high $\Delta D$ value and high adsorption amount (absolute value of $\Delta f$ is 37.2 Hz) of combining SW3, along with the sufficient adsorption density and high viscoelastic softness of the interface layer, have a crucial value for the development of Pickering emulsions and low-fat cream. Wang et al. (2023) also found that an increase in $\Delta f/n$ of the sample implies a higher adsorption rate[43].

The thickness of the interface layer is also an important factor affecting the stability of the Pickering emulsion. The $\Delta D - \Delta f$ graph is widely used for qualitative analysis of the adsorption layer. To obtain valid information about the conformational changes at the interface and the thickness of the interfacial layer, we drew the $\Delta D - \Delta f$ graph (Fig. 6D), which is called the "fingerprint graph"[44]. Generally, a smaller slope value of the curve indicates a relatively rigid and thin adsorption layer, while a higher slope value reflects viscoelasticity and a thicker layer. The thickness of the adsorption layer of SPI and WPI is 0.24 ± 0.01 and 5.31 ± 0.02 nm, respectively (Fig. 6C). The membrane thickness of the dimeric composite nanoparticles, especially the SW3 sample, is (7.24 ± 0.01 nm), which is thicker than the membrane thickness of other composite nanoparticles and single protein nanoparticles ($p < 0.05$). Combined with the high adsorption capacity of SW3 (large $\Delta f$), this indicates that the SW3 dimeric system formed a thicker adsorption layer at the interface. The thicker and harder the adsorption layer around the oil droplets in the emulsion, the stronger the spatial repulsion, thereby improving its anti-aggregation performance, which is more conducive to the formation of a stable Pickering emulsion[43].

### Stability analysis of Pickering emulsion

The storage stability of the emulsion is the main factor to evaluate the quality of the emulsion. The emulsion formation index (CI) reflects the storage stability of the emulsion[29]. The SPI emulsion had the highest CI throughout the storage process, reaching 58% on the 9th day, indicating poor stability

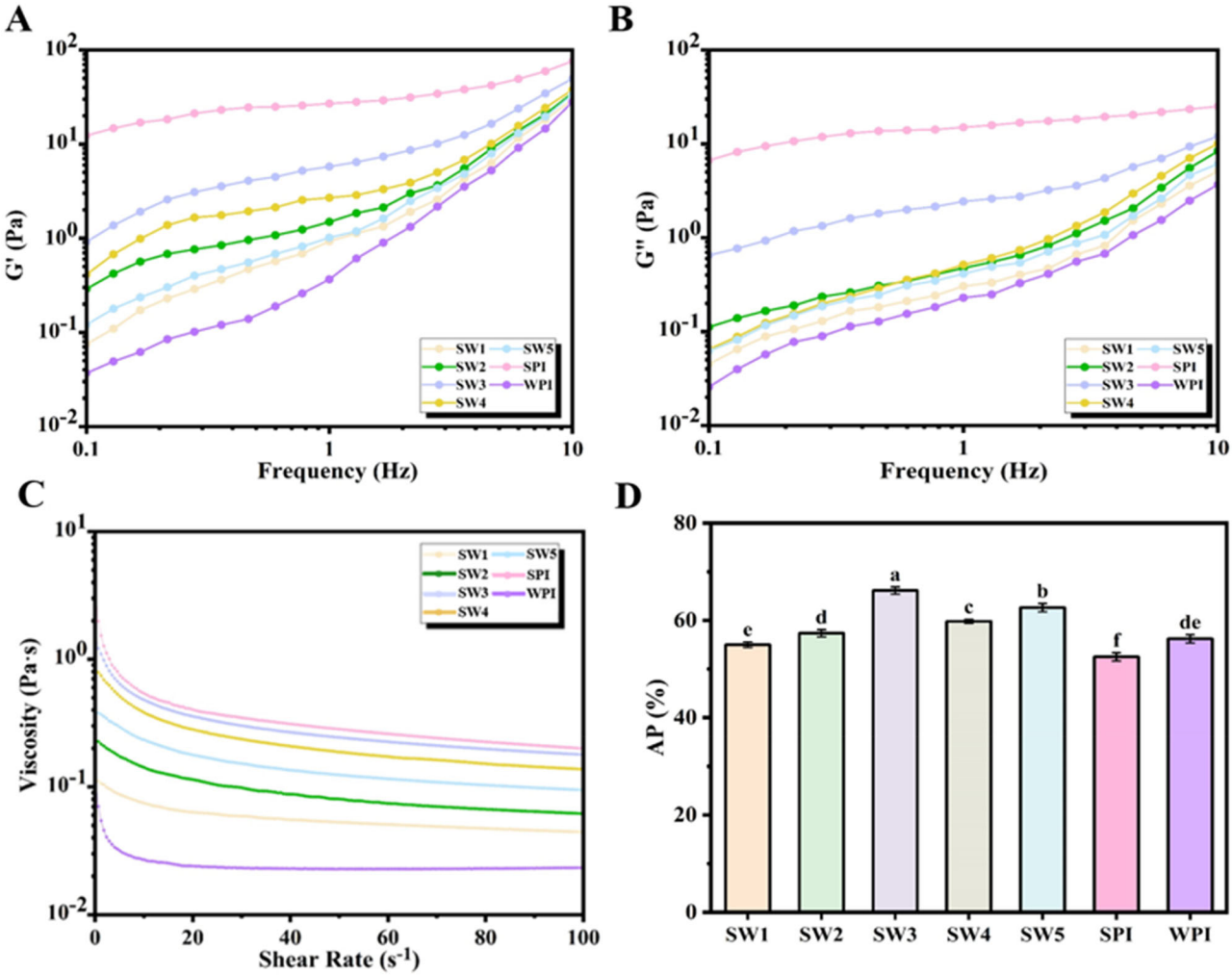


**Fig. 5 | The microscopic stability of Pickering emulsion stabilized by composite nanoparticles.** Storage modulus ($G'$) (**A**), Loss modulus ($G''$) (**B**), apparent viscosity (**C**), and adsorbed protein (**D**). All the values are expressed as mean ± SD. Mean values with different letters are significantly different ($p < 0.05$). SW1: Ultrasonic (0 W)—laccase-modified SPI cross-linked WPI; SW2: Ultrasonic (150 W)—laccase-modified SPI cross-linked WPI; SW3: Ultrasonic (300 W)—laccase-modified SPI cross-linked WPI; SW4: Ultrasonic (450 W)—laccase-modified SPI cross-linked WPI; SW5: Ultrasonic (600 W)— laccase-modified SPI cross-linked WPI; SPI soy protein isolate, WPI whey protein.

and extensive droplet aggregation (Fig. 7A). From 0 to 9 days, the CI values of each emulsion gradually increased. The CI value of the emulsion stabilized by composite nanoparticles was significantly lower than that of the emulsion in the SPI group, especially the CI value of SW3 was the lowest (the CI value on the 9th day was only 6.3%). This is because, compared with the single SPI group, the composite nanoparticles bond more tightly, forming smaller and more uniform droplets, increasing the total interface area available for stability, which is conducive to the formation of a denser and more cohesive emulsion system. Meanwhile, the increase in the surface charge of the composite nanoparticles promotes more particles to be adsorbed onto the oil–water interface, participating in the interface stability, making the emulsion have a stronger viscoelastic film and a higher interface pressure, and improving the interaction between droplets[45].

Thermal stability is essential for emulsion quality. Figure 7B and C exhibited the particle size distribution and potential changes of the emulsion after heating (37, 50, 80, and 100 °C). Compared with the emulsions of SPI and SW1 groups, the particle size of the emulsions of SW2–SW5 groups decreased significantly after heating. With the increase of heat treatment temperature, the droplet size of the emulsion increases, and the number of droplet interaction sites decreases. This observation is consistent with Guo et al. (2024), who found that the droplet size of emulsions stabilized by cannabis protein-polysaccharide complexes increased to some extent due to heat treatment-induced droplet aggregation in emulsions[46]. When treated at 100 °C, the particle size of the SW3 emulsion was 31.69 ± 1.28 μm, the emulsion separation degree was the smallest, and the emulsion separation was also significantly improved. The particle size change of the SW3 group was not significant at each temperature, indicating good stability. Heating treatment destroys the emulsion stability to a certain extent, resulting in the aggregation of emulsion droplets. SW3 also exhibited the highest absolute value of Zeta potential, further indicating that the SW3 group of emulsions has higher stability.

The ionic stability of emulsions is one of the most important indicators for evaluating the characteristics of emulsions. As depicted in Fig. 7D and E, when the concentration of NaCl increased (100–400 mM), the particle size first increased and then decreased, confirming that the presence of NaCl enhanced the interaction between protein particles. In high-concentration salt ions, composite nanoparticles may undergo structural rearrangement to form denser nanoparticles, especially SW3. The possible reason is that as the ionic strength increases, the absolute value of the zeta potential of the emulsion decreases (Fig. 7C), and the electrostatic repulsive force between the droplets weakens. Compared with the single SPI protein, the salt ion stability of the composite nanoparticles is significantly improved. When the salt ion concentration was 200 mM, the absolute value of the Zeta potential decreased significantly, which weakens the electrostatic force between

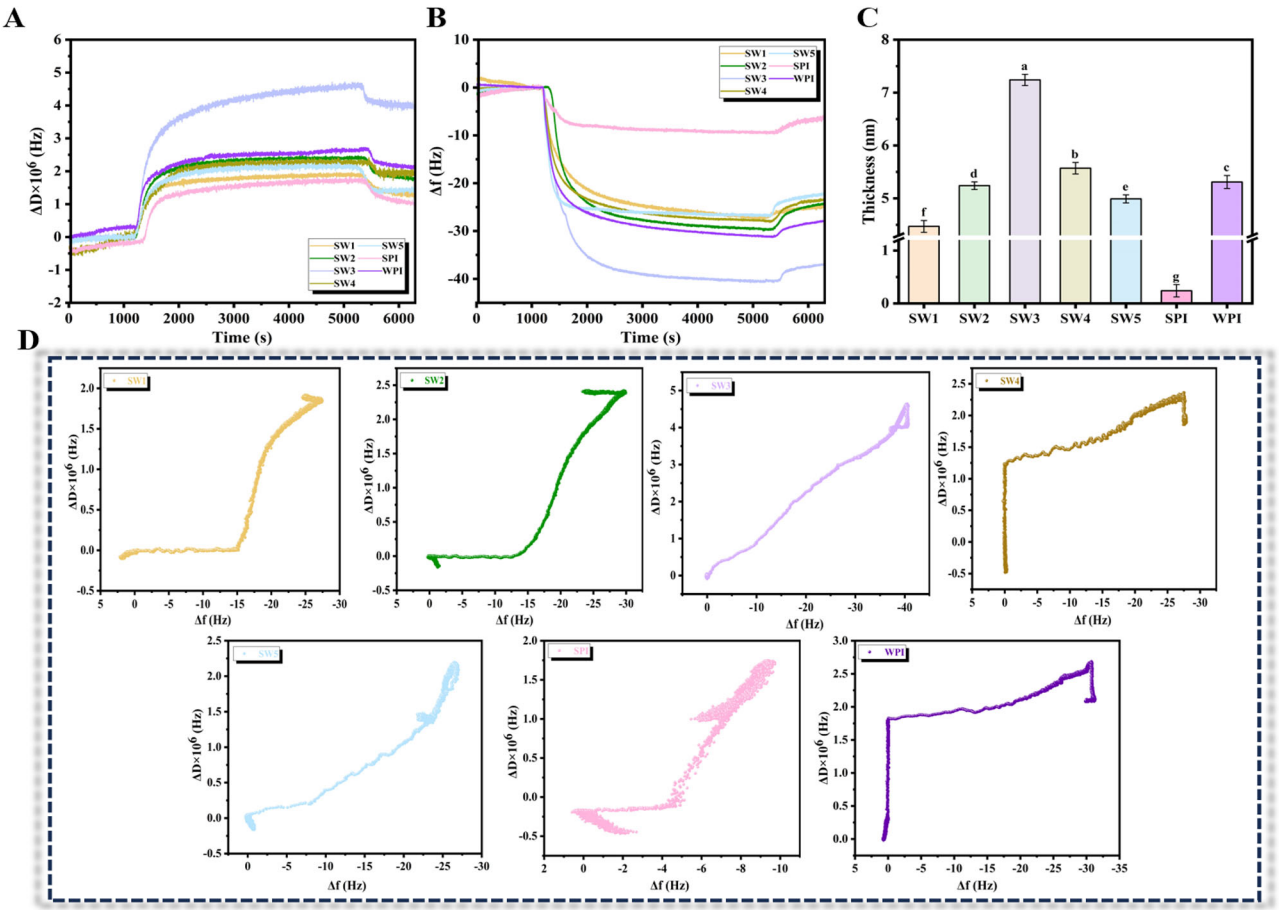


**Fig. 6 | The adsorption and assembly behavior of composite nanoparticles at the oil–water interface of Pickering emulsion.** Δ*f* (**A**), Δ*D* (**B**), adsorption film thickness (**C**), and Δ*D*−Δ*f* curves (*n* = 1 overtone) (**D**). All the values are expressed as mean ± SD. Mean values with different letters are significantly different ($p < 0.05$). Δ*f*: frequency factor; Δ*D*: dissipation factor; SW1: Ultrasonic (0 W)—laccase-modified SPI cross-linked WPI; SW2: Ultrasonic (150 W)—laccase-modified SPI cross-linked WPI; SW3: Ultrasonic (300 W) - laccase-modified SPI cross-linked WPI; SW4: Ultrasonic (450 W)—laccase-modified SPI cross-linked WPI; SW5: Ultrasonic (600 W)—laccase-modified SPI cross-linked WPI; SPI soy protein isolate, WPI whey protein.

emulsions and leads to the aggregation of emulsions. This analysis result is consistent with that of Yu et al. (2025)[47].

Centrifugal stability can reflect the ability of the emulsion to stabilize the oil phase. Unstable emulsions lead to phase separation after centrifugation[12]. Figure 7F exhibited that the centrifugal sedimentation rate of the emulsion, and the decreased Ke value indicated the enhanced stability of the emulsion. The Ke value of the emulsion stabilized by composite nanoparticles first decreased and then increased, and the centrifugal stability Ke was the lowest at SW3, which indicated that the emulsion can withstand certain centrifugal stress and has high layered physical stability. This may be attributed to the fact that more protein molecules in the SW3 emulsion system were adsorbed at the oil–water interface, thus forming a stronger gel network structure, which can effectively prevent the aggregation between droplets and enable the emulsion to maintain a better state under the condition of high-speed centrifugation.

## Microstructure of emulsion

The microstructure of Pickering's emulsion was observed by an optical microscope combined with CLSM. Figure 8 visually exhibited the micro-droplet size changes with ultrasonic intensity. There was no obvious difference in the appearance of the seven emulsion samples. Smaller drop sizes are critical because they are closely associated with enhanced emulsion stability in conventional emulsion systems[5]. Through LM observation, it was found that the droplets of the emulsion of a single SPI did not form. The emulsion stabilized by composite nanoparticles has uniform and dense droplet distribution.

Stain the same area with oil droplets and proteins with Nile red (red) and Nile blue (green). Pickering emulsion is a spherical liquid droplet with an inner oil phase and an outer water phase. It can be clearly seen that the red oil droplets are surrounded by the green protein solution (Fig. 9), indicating that the complex protein nanoparticles successfully adsorbed the oil–water interface to form a spatial barrier, effectively preventing the droplet aggregation. Due to the low particle concentration in the oil phase, the droplets of a single protein-stable emulsion are large, unevenly distributed, and have local aggregation. Stable emulsion droplets of complex protein particles form more uniformly dispersed regular spheres with smaller particle sizes. In particular, the stability of SW3 emulsion was significantly enhanced, and the spherical droplets maintained good separation without obvious flocculation. This is due to the physical force generated by moderate ultrasound that opens the structure of SPI, promotes the formation of thicker interfacial films of complex proteins, and increases the spatial resistance between droplets.

## Determination of properties of low-fat cream

During the beating process of cream, a complex foam system is formed, and its stability largely depends on the rheological properties at its interface[48]. The viscosity curve illustrates the relationship between shear rate and apparent viscosity, indicating that all creams exhibit shear thinning behavior, which is a characteristic of pseudoplastic fluids. This phenomenon makes the sample more suitable for extrusion through the nozzle of a 3D printer. As shown in Fig. 10A, the viscosities of the creams prepared by SW2, SW3, SW4, and SPI were all higher than those of the commercially available

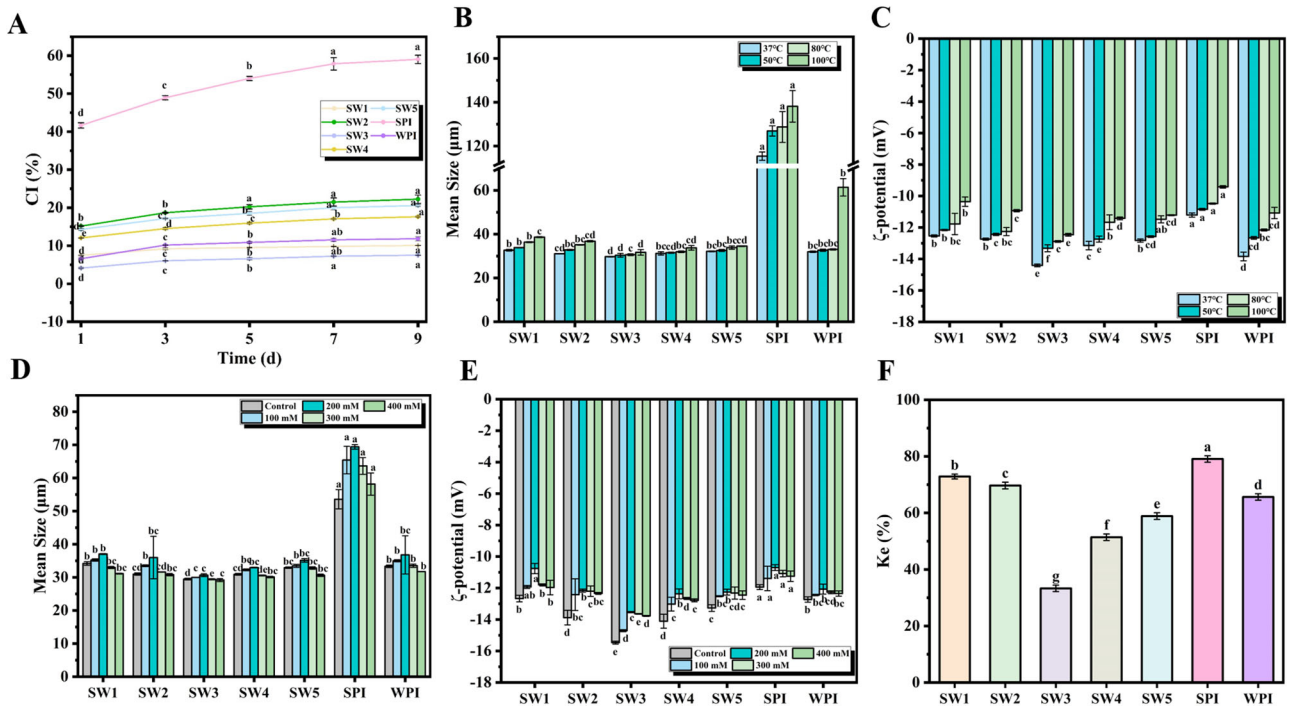


**Fig. 7 | Stability analysis of Pickering emulsion stabilized by composite nanoparticles.** CI analysis (**A**). The influence of different processing temperatures (37, 50, 80, and 100 °C) on the particle size (**B**) and potential (**C**) of the stable Pickering emulsion of composite nanoparticles. The influence of different sodium ion concentrations (100, 200, 300, and 400 mM) on the particle size (**D**) and potential (**E**) of the stable Pickering emulsion of composite nanoparticles; Centrifugal stability (**F**). All the values are expressed as mean ± SD. Mean values with different letters are significantly different ($p < 0.05$). CI: creaming index; Ke represents stability parameter; SW1: Ultrasonic (0 W)— laccase-modified SPI cross-linked WPI; SW2: Ultrasonic (150 W)—laccase-modified SPI cross-linked WPI; SW3: Ultrasonic (300 W)—laccase-modified SPI cross-linked WPI; SW4: Ultrasonic (450 W)—laccase-modified SPI cross-linked WPI; SW5: Ultrasonic (600 W)—laccase-modified SPI cross-linked WPI; SPI soy protein isolate, WPI whey protein.

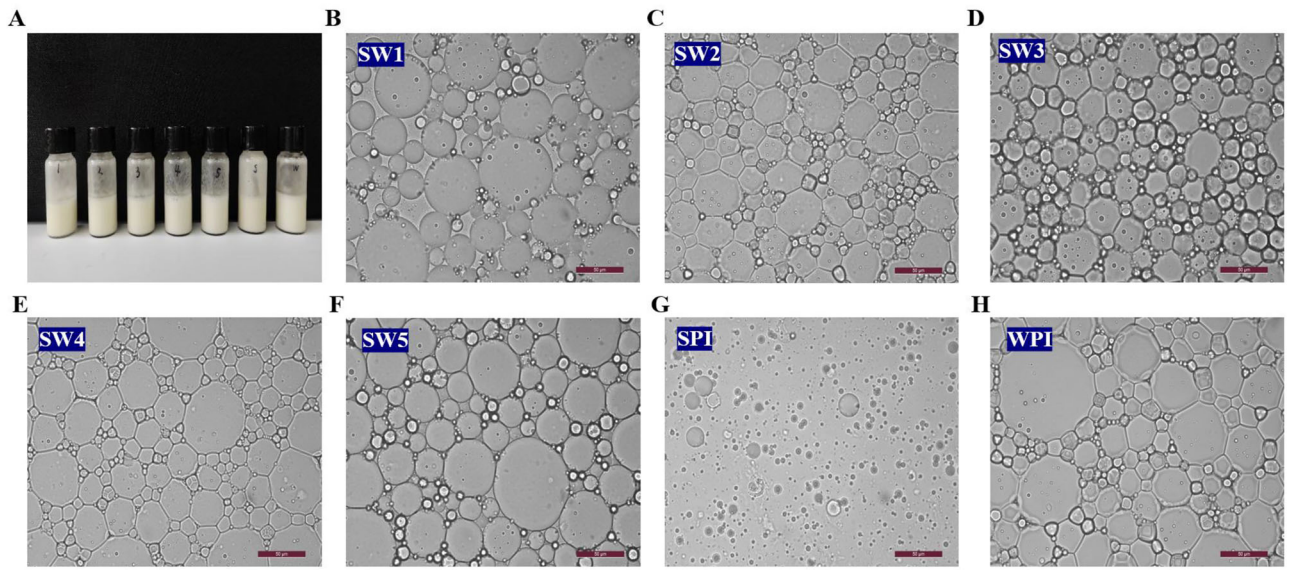


**Fig. 8 | Macroscopic stability and microscopic morphology of Pickering emulsions stabilized by composite nanoparticles.** Intuitive (**A**) and optical microscope images (**B**–**H**) of Pickering emulsion stabilized by composite nanoparticles. SW1: Ultrasonic (0 W)—laccase-modified SPI cross-linked WPI; SW2: Ultrasonic (150 W)—laccase-modified SPI cross-linked WPI; SW3: Ultrasonic (300 W)—laccase-modified SPI cross-linked WPI; SW4: Ultrasonic (450 W)—laccase-modified SPI cross-linked WPI; SW5: Ultrasonic (600 W)—laccase-modified SPI cross-linked WPI; SPI soy protein isolate, WPI whey protein.

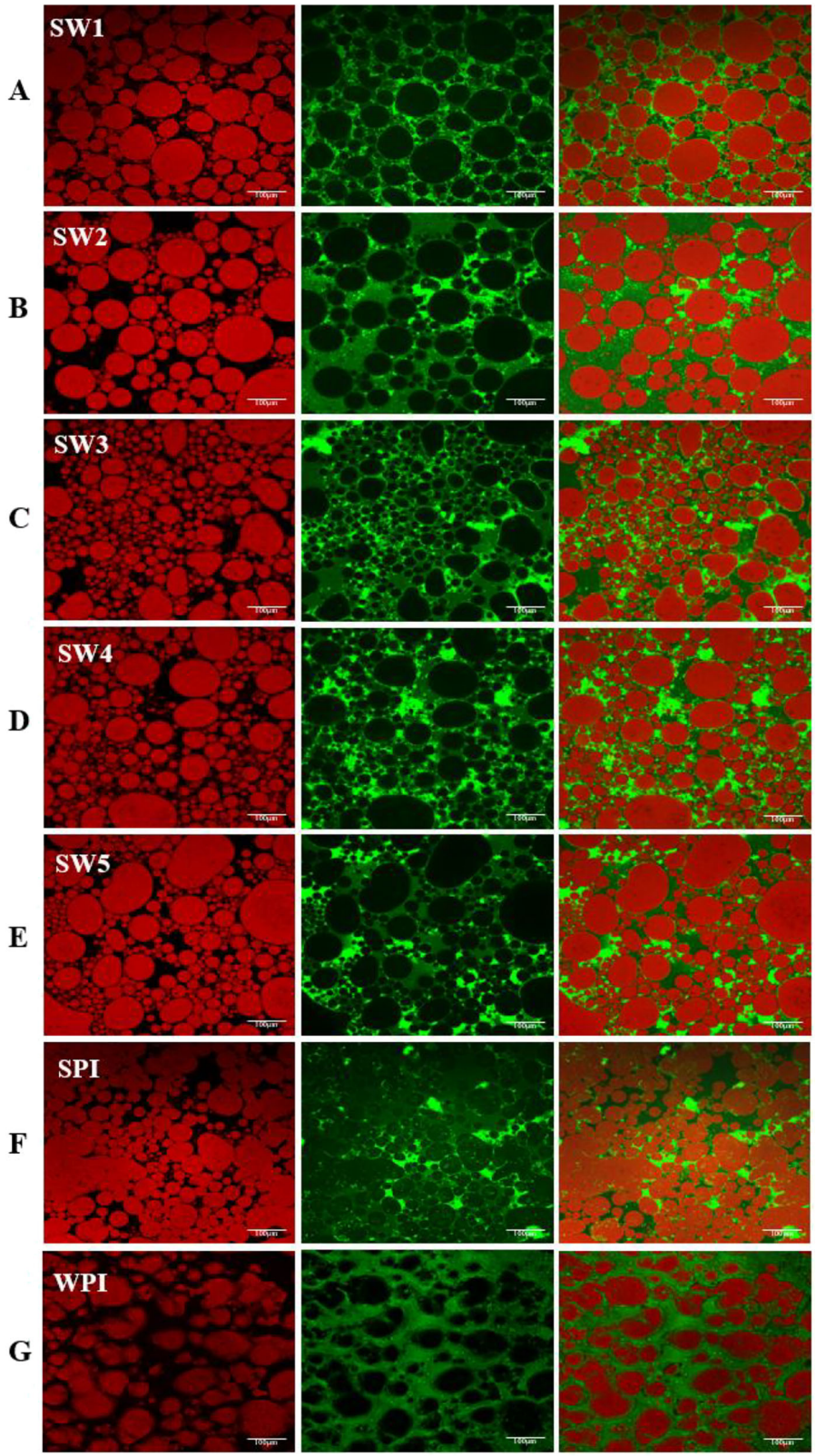


**Fig. 9 | Laser confocal microscope images of Pickering emulsion stabilized by composite nanoparticles. A–G** represents the laser confocal images of the SW1-SW5, SPI and WPI group samples, respectively. SW1: Ultrasonic (0 W)—laccase-modified SPI cross-linked WPI; SW2: Ultrasonic (150 W)—laccase-modified SPI cross-linked WPI; SW3: Ultrasonic (300 W)—laccase-modified SPI cross-linked WPI; SW4: Ultrasonic (450 W)—laccase-modified SPI cross-linked WPI; SW5: Ultrasonic (600 W)—laccase-modified SPI cross-linked WPI; SPI soy protein isolate, WPI whey protein.

vegetable cream and WPI groups. Among them, the cream prepared by SW3 has the highest apparent viscosity. This might be due to the increase in the number of hydrogen bonds formed between the SW3 group of composite nanoparticles and water, the increase in shear resistance, and viscosity. Atik et al. (2021) also reported that replacing milk fat with the by-product of cold-pressed chia seed oil resulted in the low-fat ice cream exhibiting shear-thinning flow characteristics[49]. Meanwhile, the size of particle size also has a significant impact on the apparent viscosity of the emulsion. Under the condition that the volume fraction of the dispersed phase is the same, the smaller the particle size of the samples in group SW3 is, the interaction between fat globules enhances, and the apparent viscosity of emulsification increases[50].

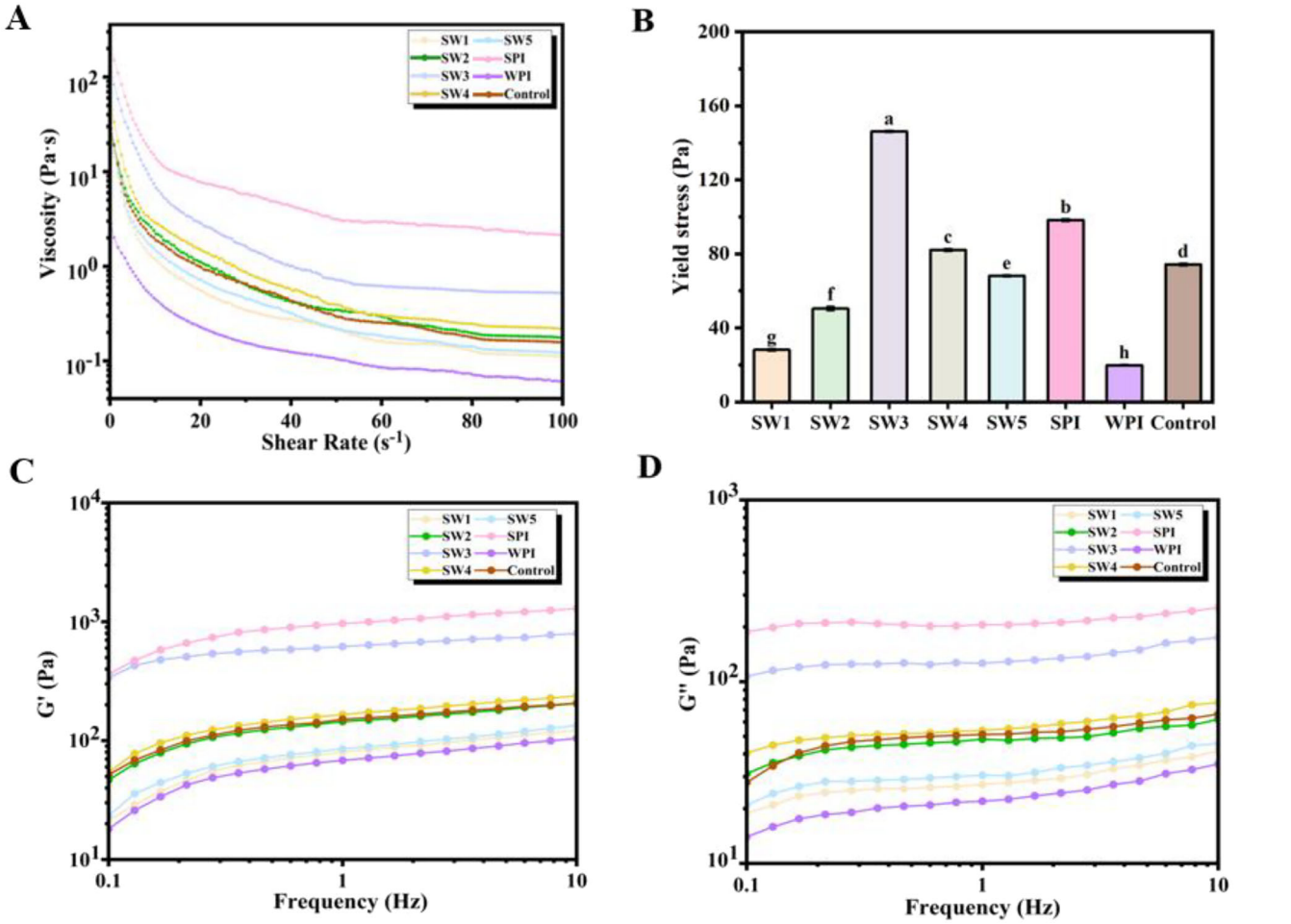


**Fig. 10 | Determination of rheological properties of low-fat cream.** Surface viscosity (**A**), yield stress (**B**), elastic modulus $G'$ (**C**), and viscous modulus $G''$ (**D**). All the values are expressed as mean ± SD. Mean values with different letters are significantly different ($p < 0.05$). The Control group was the commercially available plant-based cream group; SW1: Ultrasonic (0 W)—laccase-modified SPI cross-linked WPI; SW2: Ultrasonic (150 W)—laccase-modified SPI cross-linked WPI; SW3: Ultrasonic (300 W)—laccase-modified SPI cross-linked WPI; SW4: Ultrasonic (450 W)—laccase-modified SPI cross-linked WPI; SW5: Ultrasonic (600 W)—laccase-modified SPI cross-linked WPI; SPI soy protein isolate, WPI whey protein.

Yield stress is the critical point of rheological behavior. When the yield stress is within the range of 100–200 Pa, it can not only ensure the moderate extrusion resistance required by the cream, but also maintain sufficient structural strength to keep the integrity. If the stress is too small, the formability will be poor. Chakraborty et al. (2025) also researched that the increase in yield stress indicated the formation of a more solid structure and a more stable emulsion, representing a more uniform particle volume and enhanced flow characteristics[51]. As shown in Fig. 10B, the SPI yield stress was 98.3 Pa. The yield stress of the cream prepared by SW1-3 gradually increased, which were 28.19 ± 0.70, 50.42 ± 1.20, and 146.22 ± 0.57 Pa, respectively. Especially, the cream prepared by the SW3 group had the best effect. The partially aggregated fat in the cream prepared by SW4 and SW5 decreased, and the yield stress dropped to 82.15 ± 0.81 Pa and 68.12 ± 0.55 Pa, respectively, showing that the cream texture was relatively soft.

The energy storage modulus ($G'$) and the loss modulus ($G''$), respectively, represent the contributions of elasticity and viscosity. Figure 10C and D revealed that as the frequency increases, the $G'$ of the whipped cream gradually increases, showing a clear frequency dependence, and $G'$ was always greater than $G''$, indicating that the elastic characteristics of the whipped cream were higher than the viscous characteristics, and it has the performance of a gel system. The frequency scan $G'$ value of the cream prepared by SW4 and SW5 decreased, and the change in frequency scan after whipping the cream was consistent with the trend of viscosity change.

The aggregation of some fats has a significant impact on the structural formation of whipped cream. Previous studies have also revealed that the higher the fat coagulation rate, the more conducive it is to the formation of a stronger foam system[52]. The evaluation of the coalescence rate of the fat part using different composite nanoparticles as alternative fats in the preparation of cream (Fig. 11A). The results exhibited that the fat coagulation rate in the cream of all composite nanoparticle groups was significantly increased ($p < 0.05$) compared with the SPI group. It is indicated that appropriate ultrasonic treatment induced the spatial structure of the composite protein and enhanced the emulsification foaming performance of the system. The excellent foaming performance of the SW3 group samples promoted the formation of smaller bubbles in the emulsion during the heating process, thereby increasing the area of the bubble film and promoting the partial polymerization of fat globules.

Hardness is an assessment of the ability of cream to maintain its foamy shape and stability after being whipped. It is closely related to the coalescence rate of the fat part and the concentration of interface proteins[53]. As shown in Fig. 11B, the hardness of the cream in the SW2–SW5 group was significantly higher than that in the SPI group and the Control group. The hardness of the cream in the SW3 group (79.34 g) was significantly higher than that in the SW1 group (61.00 g) ($p < 0.05$). This might be due to the high degree of fat agglomeration and dense agglomeration network in the cream of the SW3 group. The high concentration of interface proteins makes the cream foam structure of the SW3 group firmer and increases its

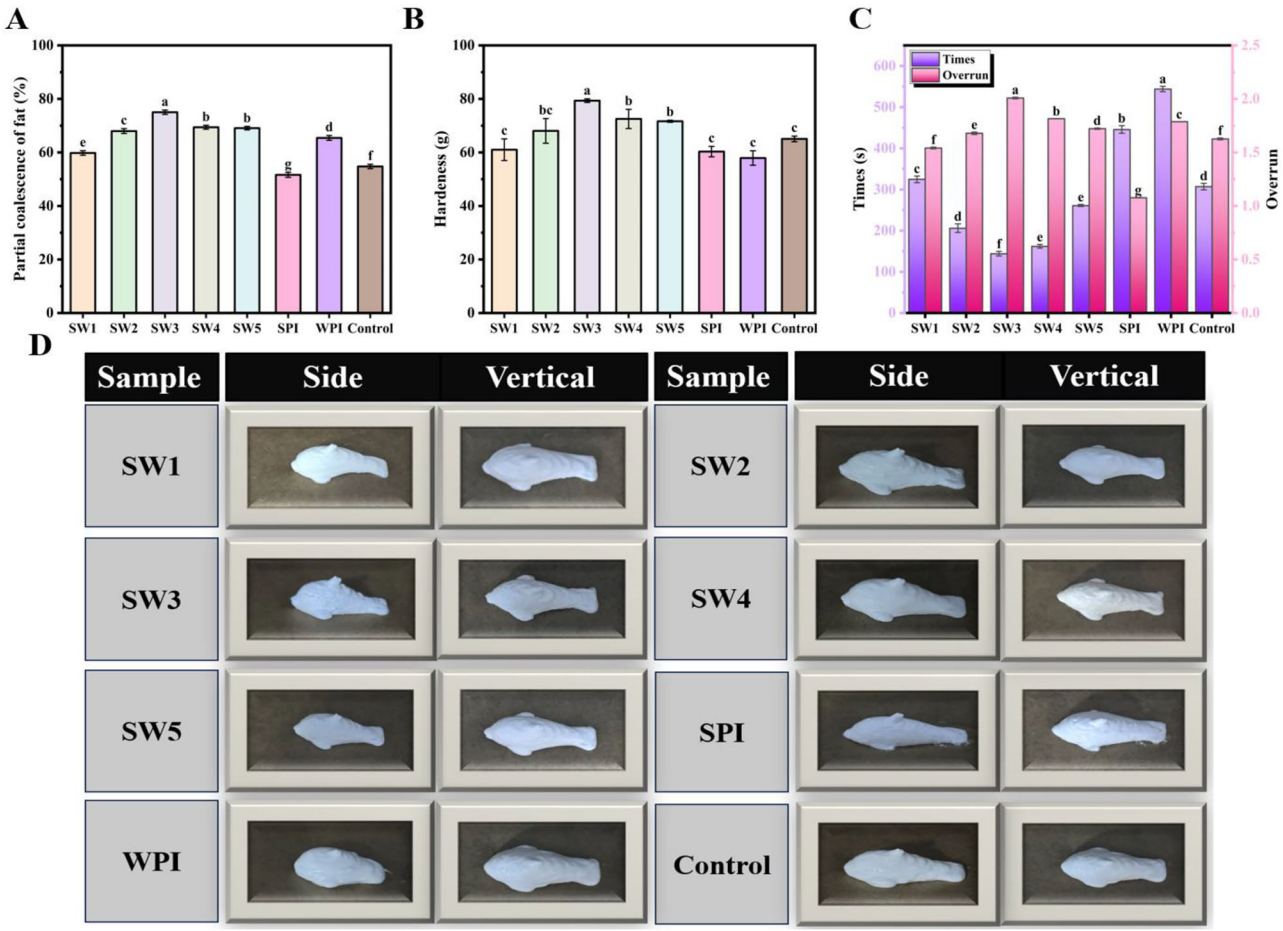


**Fig. 11 | Evaluation of physical and quality properties of low-fat cream.** The fat partial coalescence rate (**A**), hardness (**B**), whipping foaming rate (**C**) and 3D printing (**D**) of low-fat cream. All the values are expressed as mean ± SD. Mean values with different letters are significantly different ($p < 0.05$). The Control group was the commercially available plant-based cream group; SW1: Ultrasonic (0 W)—laccase-modified SPI cross-linked WPI; SW2: Ultrasonic (150 W)—laccase-modified SPI cross-linked WPI; SW3: Ultrasonic (300 W)—laccase-modified SPI cross-linked WPI; SW4: Ultrasonic (450 W)—laccase-modified SPI cross-linked WPI; SW5: Ultrasonic (600 W)—laccase-modified SPI cross-linked WPI; SPI soy protein isolate, WPI whey protein.

hardness. Han et al. (2023) demonstrated that proteins can provide a more elastic and resilient texture compared to liquid fats, thereby enhancing the overall hardness of the cream[9]. Compared with the SW3 group, the hardness of the cream in the SW4 and SW5 groups was significantly decreased ($p < 0.05$). This was due to the particle aggregation in the SW4 and SW5 groups and the loose internal structure of the composite nanoparticles, resulting in a decrease in hardness.

The formation and stability of the foaming system are crucial to the texture of cream. The foaming rate during whipping is an effective means to evaluate the ability of the emulsion to wrap bubbles. As shown in Fig. 11C, the whipping foaming rate and whipping time of the cream prepared by different sample groups with different treatments are inconsistent. Compared with the SPI group, the foaming rate of cream whipping in the other groups increased significantly. In particular, the SW3 group increased by 93.15% compared with the SPI group ($p < 0.05$). This might be since the composite nanoparticles have a better foaming ability and can effectively encapsulate the bubbles. Qian et al. (2025) demonstrated that the apparent viscosity of fresh cream is directly related to the foaming process. The greater the apparent viscosity, the more difficult it is to fill air during the foaming process, and the smaller the bubble volume[54]. The beating times of the SPI, WPI, and commercial cream groups were 445.67 ± 9.29, 544.00 ± 6.56, and 308.00 ± 7.93 min, respectively. The beating time of the cream in the SW3 group was significantly reduced to 144.00 ± 5.57 min ($p < 0.05$).

3D printing materials based on extrusion methods need to have good extrudability and consistency. In this study, the shape retention and structural stability of whipped cream prepared by composite nanoparticles were verified through a three-dimensional "dolphin" model. As shown in Fig. 11D, during the extrusion stage of printing, all groups of cream can be continuously and smoothly extruded from the nozzle and quickly deposited on the printing platform. The SPI group and SW2–SW4 group cream are close to the preset model height and shape. Especially, the SW3 group model has no obvious collapse, the surface texture is clear, the precision is accurate, and it has good forming stability. Compared with the single 3D model of protein-based cream extrusion, the low-fat cream prepared from SW3 emulsion has a high viscosity and foaming rate, and also features stable, strong, and high printing performance. The viscosities of the WPI, SW1, and SW5 groups decreased, showing obvious edge collapse, indicating that they are not suitable for printing complex structures. This is because its viscosity is relatively low, and the prepared cream is difficult to quickly recover from the liquid state to the semi-solid state during frequent extrusion movements, which is consistent with the results of low $G'$, $G''$ values, and apparent viscosity in previous rheological studies.

## Discussion

In this study, SPI was treated with different intensities of ultrasound combined with laccase modification. A dual-protein system was constructed by combining WPI to prepare low-fat Pickering cream. The microstructure, rheological properties, and interface adsorption characteristics of the composite nanoparticles stabilizing the Pickering emulsion were evaluated using multi-scale (microscopic, macroscopic, and molecular) methods,

achieving functional enhancement and stability in the cream preparation. The results revealed that the stable emulsion of SW3 (300 W) had the best interface performance, capable of forming an oil–water interface film and maintaining droplet dispersion. The interface adsorption protein content of this group of emulsions was higher, and its CI value was 4.81% on the 9th day of storage, demonstrating good storage stability. Meanwhile, the fat coalescence rate of the low-fat cream based on SW3 was as high as 75.01%, which was higher than that of the plant-based cream on the market. The addition of dual-protein nanoparticles also enhanced the self-supporting performance of the 3D printing samples of Pickering cream, especially SW3, with high printing accuracy and smooth surface texture. The research results provided a basis for the development of low-fat and low-calorie cream products. However, this study was based on a single oil phase to clarify the inherent advantages of the stable Pickering emulsion stabilized by dual-protein particles in low-fat cream. Future research needs to further explore the ratio of a single oil phase to milk fat, clarify the emulsification stability of the emulsion stabilized by dual-protein complex particles in the mixed oil phase, and lay the foundation for the further expansion of the oil phase in low-fat cream.

## Materials and methods

### Materials

SPI was purchased from Shandong Wandefu Biotechnology Co., Ltd. (Shandong, China), and soybean oil was purchased from Jiusan Grain and Oil Industry Group Co., LTD. Laccase was obtained from Sigma-Aldrich Company (USA). All other experimental reagents used are of analytical grade.

### Selection of the compounding ratio of SPI and WPI

SPI and WPI were respectively dissolved in deionized water to achieve a final concentration of 5% (m/v), and then hydrated overnight. Subsequently, the mixture was thoroughly stirred in different proportions of SPI: WPI (5:0, 3:1, 1:1, 1:3, and 0:5). The pH of the mixture was adjusted to 7.0. Then it was stored at −80 °C until it was freeze-dried. Before testing, all the samples were suspended in deionized water at a final concentration of 1 mg/mL. The sample was balanced at 25 °C for 120 s and measured by particle size and potential analyzer (Malvern Instruments, Nano-ZS90, UK). Each sample was measured three times, and the average value was taken. The microstructure of the samples was taken with SEM (Hitachi, Japan). The freeze-dried samples were pasted on the copper sample rack, and the surface was treated with gold spray, and the apparent morphology was observed at an acceleration voltage of 5 kV times[1]. The relevant experimental results can be found in the supplementary materials.

### Preparation of modified soybean protein isolate (MSPI)

According to the previous research method and with appropriate modifications[55], SPI modified by laccase with different ultrasonic powers were prepared. Briefly, SPI was dispersed in deionized water (solid–liquid ratio 8 g/100 mL), stirred at 25 °C for 2 h using a magnetic stirrer, and placed in a refrigerator at 4 °C for full hydration overnight. The probe of the ultrasonic cell crusher was inserted into the SPI dispersion solution and treated at 2 cm below the liquid level for 30 min at ultrasonic powers of 0, 150, 300, 450, and 600 W, respectively. The working time was 4 s, and the intermittent recovery time was 5 s. During ultrasonic processing, the sample should be placed on crushed ice. Then, the pH value of the protein solution after ultrasound was adjusted to 6.5, and laccase (35 U/g) was added and heated in a water bath at 30 °C for 6 h. After the reaction, the sample was placed in a constant temperature water bath at 75 °C to deactivate the enzyme for 15 min. The samples were freeze-dried and stored for subsequent experiments.

### Preparation of MSPI–WPI composite nanoparticles and Pickering emulsions

Dilute MSPI with deionized water to a final concentration of 5% (m/v). Mix the WPI solution (5%, m/v) at the same concentration in a 1:1 ratio with the MSPI solution, and stir thoroughly. Perform two homogenization treatments under a pressure of 30 megapascals to obtain a dispersed solution. Pre-cool the solution at −20 °C, and then conduct vacuum freeze-drying. Based on the different intensities of MSPI ultrasonic treatment (0, 150, 300, 450, 600 W), the combined nanoparticles are respectively named SW1–SW5.

The preparation of Pickering emulsion follows the process described by Türker (2025)[5]. A suspension of double protein nanoparticles dissolved in deionized water is mixed with the oil phase (accounting for 60% of the total volume). Then, homogenization was carried out using the T18 IKA homogenizer (IKA Werke, Germany) with high-speed shear of 10,000 rpm for 3 min. The visual appearance of the emulsion was monitored by placing 15 mL Pickering emulsions in equal parts under different conditions in 20 mL lidded bottles, and the remaining samples were tested for microstructure and stability.

### Characterization of composite nanoparticles

Based on the previous research method and slightly modified[56]. The samples were resuspended in deionized water to a final concentration of 0.2 mg/mL. The absorption spectrum of the sample was measured by a UV-2600 ultraviolet visible spectrophotometer (Shimadzu Instrument Co., LTD, Japan). The scanning wavelength was 200–400 nm with medium speed. All the samples were suspended in deionized water at a final concentration of 0.2 mg/mL, and the fluorescence intensity of the sample was determined by a fluorescence spectrophotometer (RF-6000, Shimadzu, Japan) at the excitation wavelength of 280 nm. The measurement parameters also include a slit width of 5 nm and an emission spectrum wavelength range of 300–480 nm[57]. The samples were measured by X-ray diffractometer (Bruker D8 Advance, Germany) equipped with Cu Kα radiation source ($\lambda$ = 1.5418 Å). The operating conditions were as follows: scan speed at 5°/min was operated at 40 kV/40 mA. The scanning range of wide-angle X-ray diffraction figure $2\theta$ ranging from 5° to 60° [58].

With a slight modification of the previous method[59], the solubility of the sample in different buffers was measured. 0.3 g sample was mixed with 0.3 mL of four different solvents and then homogenized using a homogenizer at 1000 rpm. The mixture was then centrifuged at 10,000 × $g$ for 10 min after standing for 2 h. The protein concentration in the supernatant was determined by the BCA method. The four denaturing solutions were: 0.06 M NaCl (S1), 0.6 M NaCl (S2), 0.6 M NaCl + 1.5 M urea (S3), 0.6 M NaCl + 8 M urea (S4), and 0.6 M NaCl + 8 M urea + 0.5 M dithiothreitol (DTT) (S5). Protein concentration of different solutions corresponding to the ionic bond (S2 and S1), hydrogen bonding (S3 and S2), hydrophobic interactions (S4 and S3), and the disulfide bond (S5 and S4).

The changes in interfacial tension between the sample and soybean oil over time (3600 s) were detected by an OCA 20 AMP analyzer (Data Physics Instruments, Germany). To make the interfacial tension–time curve steady gradually, the measurement time was 3600 s by the dynamic suspended drop method[29].

The three-phase contact angle of the sample was determined using an OCA 20 AMP analyzer (Data Physics Instruments, Germany). Briefly, the composite nanoparticles were formed into a round sheet with a thickness of about 1 mm and a diameter of about 10 mm, which was placed on the slide. 5 μL (1 drop) ultra-pure water was deposited on the surface of the wafer by the seat drop method. After the water droplets were balanced on the surface of the wafer, continuous recording and observation were carried out.

### The microscopic scale of composite nanoparticles

The sample processing methods for particle size and Zeta potential are the same as those described in the section "Characterization and interaction of MSPI/WPI composite nanoparticle". The morphology of the sample solution was determined by TEM (H-7650, Hitachi, Japan) at 100 kV. Briefly, the lyophilized protein powders were resuspended in deionized water to a final concentration of 0.3 mg/mL. Then 20 μL sample was dropped on the copper net covered with PVCP film for natural drying, and then added with 20 μL tungsten phosphate solution (2%) for negative staining, placed for

2 min, and observed and photographed after the particles were completely stained.

### Evaluation of properties of nanoparticle-stabilized Pickering emulsions

The initial temperature was set at 25 °C, and the strain amplitude of the fixed dynamic frequency scan test was 1% (within the linear viscoelastic region). The oscillation frequency was set at 0.1–100 Hz, the retention time was 60 s, and the balance was 3 min before each test. The energy storage modulus $G'$ and loss modulus $G''$ of the sample within the range of frequency change were recorded[60]. The rheological properties of the nanoparticle-stabilized Pickering emulsion were evaluated using a Haake Mars 40 rheometer (Thermo Fisher Scientific, Waltham, MA, USA) with a 40 mm parallel plate. Under the condition of 25 °C and 1% strain, the apparent viscosity of protein samples was determined at the shear rate of 0.1–100 $s^{-1}$ for 5 min.

Centrifuge 5 mL of emulsion (10,000 × *g*; 30 min), the bottom clear solution was collected, and the protein content of the supernatant was determined by the BCA method[44].

$$AP(\%) = \frac{C_0 - C_s}{C_0} \times 100 \quad (1)$$

where $C_0$ is the initial protein concentration of the emulsion. $C_S$ is the protein concentration in the supernatant.

### Quartz crystal microbalance (QCM)

Refer to the previous research methods and make appropriate modifications[44]. The adsorption and desorption of composite nanoparticles at the interface were measured using a Q-Sense instrument (Q-Sense, Biolin, Sweden). Initially, a mixed vegetable oil film was introduced by spreading 200 μL soybean oil–chloroform solution (0.5%, v/v) onto the gold sensor (QSX 301, 5 MHz) and drying the coated sensor at 37 ± 0.2 °C for 12 h. Before each coating, the gold sensor was cleaned in a water bath with a mixed solution (prepared by mixing ultra-pure water, ammonia, and hydrogen peroxide at a volume ratio of 5:1:1) at 75 °C for 15 min. The gold sensor was dried using nitrogen to completely remove the oil and composite nanoparticles, allowing for recovery.

Initially, the sensor was rinsed with ultra-pure water for 30 min to calibrate the quasi-equilibrium baseline, and then the composite nanoparticle solution (0.5 mg/mL) was adsorbed to the surface of the sensor for 70 min. Finally, the electrodes were flushed again with ultra-pure water to wash away any unbound or loosely bound molecules. Real-time shifts in frequency ($\Delta f$) and dissipation ($\Delta D$) were recorded. All experiments were performed at 25 ± 0.5 °C at a flow rate of 40 μL/min.

### Stability of Pickering emulsions stabilized by composite nanoparticles

The emulsions were sealed in 10 mL glass bottles (inside diameter 2.5 cm, height 7.0 cm) and stored at 4 °C. The CI values of the emulsion were measured at the 1st, 3rd, 5th, 7th, and 9th days. This index was calculated from Eq. (2)

$$CI(\%) = \frac{H_s}{H_t} \times 100 \quad (2)$$

where CI represents cream index; $H_s$ and $H_t$ represent the recorded height of the emulsion precipitation layer and the total height of the emulsion, respectively.

10 mL emulsions were added into the glass bottle, heat treated at 37, 50, 80, and 100 °C for 30 min, and stored at room temperature for one day. The average droplet size and potential of the emulsion were measured.

The Pickering emulsion was dispersed in aqueous solution with different ionic strength $Na^+$ concentrations (0, 100, 200, 300, 400 mmol/L). Then, the average droplet size and potential of the emulsion were measured after 30 min of equilibrium[46]. Briefly, dilute the emulsion with deionized water 100 times. Then, measure the particle size and potential of the emulsion droplets using the method described in "Quartz crystal microbalance (QCM)". The refractive indices of the oil phase and water phase are 1.470 and 1.330, respectively.

Centrifugal stability was assessed using a modified method from a prior study[29]. Suck 40 μL emulsion from the bottom of the container, dilute the emulsion with 4 mL 0.1% (w/v) SDS solution, mix and centrifuge for 5 min (5000 r/min), and measure the absorbance value at 500 nm. The centrifugal stability constant (Ke) of the emulsion is calculated as follows:

$$Ke(\%) = \frac{A_0 - A}{A_0} \times 100 \quad (3)$$

where $A_0$ is the absorbance of the emulsion before centrifugation, and $A$ is the absorbance of the emulsion after centrifugation.

### Light microscope

Morphological images of Pickering emulsions were captured using a BX53 optical microscope (Olympus Corp., Tokyo, Japan) so that their structural features could be examined.

### Confocal laser scanning microscopy (CLSM)

A model FV 1200 microscope (Olympus Corp., Tokyo, Japan) was used to analyze the microstructure of emulsions. The oil phase and the water phase were stained respectively with 0.1 wt% Nile red and Nile blue (dissolved in isopropyl alcohol). 1 mL of the sample was mixed with 20 μL Nile red and 20 μL Nile blue, and after being evenly mixed, it was stained overnight away from light. The 5 μL sample was uniformly dropped on the slide and placed on the stage for observation. The laser wavelengths of Nile Red and Nile Blue A are 488 and 633 nm, respectively.

### Preparation of low-fat cream

Refer to the previous method and make slight modifications to prepare cream[48]. Modify the commercial fresh cream emulsion formula, with the components including 25% hydrogenated palm oil, 1.08% sodium lactate, xanthan gum 0.2%, white granulated sugar 15%, sucrose syrup 7.5%, D-sorbitol 0.95%, and 50.7% water. Use the Pickering emulsion prepared from MSPI–WPI complex protein nanoparticles with different intensities of treatment to replace the hydrogenated palm oil. Mix all the components in proportion, raise the temperature to 75 °C, and stir. Homogenize the mixture at 10,000 revolutions per minute (IKA homogenizer from Stauben, Germany) for 2 min. Then immediately refrigerate, and refrigerate at 4 °C for 24 h before whipping or analysis. The cream maintains a temperature below 10 °C during whipping.

### Assessment of the characteristics of low-fat cream

The rheological properties of the cream were tested using a rheometer with a stainless-steel parallel plate clamp (diameter 40 mm, clearance height 0.06 mm). After the rheometer was corrected, the cream was added to the stage, and the formal experimental test was carried out after 180 s of equilibrium at 10 °C. The apparent viscosity and yield stress were measured, and the scanning mode shear rate from 0.1 to 100 $s^{-1}$ was recorded. Under the condition of the strain condition of 0.5%, were recorded in the 0.1–10 Hz oscillation frequency scanning mode determination of storage modulus $G'$ and loss modulus $G''$.

Take a mixture of 10 g of cream and 5 g of oil red O solution, and centrifuge it at 8000 × *g* at 25 °C for 30 min. After centrifugation, stand for 10 min, remove the clear and transparent red oil from the upper layer, and pour it into the colorimetric dish to measure the absorbance at 520 nm. Taking corn oil (without oil red O) as the control, the absorbance of the dye solution at 520 nm was determined. The calculation formula is as follows:

$$\Phi = \frac{M_1 \times (\alpha - 1)}{M_2 \times \psi} \quad (4)$$

where Φ (%) is the coalescence rate of the fat part, $M_1$ (g) is the mass of the oil red O solution added, $\alpha$ (dimensional) is the absorbance ratio of the oil red O solution before and after centrifugation, $M_2$ (g) is the mass of the cream, and Ψ (w/w%) is the mass fraction of the fat in the cream.

The hardness of low-fat cream was determined by the TA-XT2i texture analyzer (Stable Microsystems, UK). Measurement parameters: *P*/0.5 probe, measured the pressure mode, the trigger force was 5 g, the probe speed before, during, and after the test is set to 5.0, 1, 5 mm/s, the test distance is 25 mm[61].

Remove 200 g frozen emulsion after 24 h of refrigeration and thawing, heat up with cold water to 0–2 °C, pour the emulsions into a mixing tank cooled at 4 °C, and use a whisk to beat until the end of the beating. The formula for determining whipping foaming rate was as follows:

$$WFR\,(\%) = \frac{m_1 - m_2}{m_2} \times 100 \quad (5)$$

where $m_1$ is the mass of the same volume of unbeaten emulsion, g; $m_2$ is the same volume as the mass of the beaten emulsion, g.

The Pickering emulsions were printed using a FOODBOT-S2 extrusion printer (Hangzhou Shiyin Technology, Hangzhou, China)[62]. The low-fat cream sample was loaded into the 3D printer box, and the printer was preheated at a printing temperature of 20 °C for at least 15 min before printing. Printed at room temperature using an extrusion 3D printer, shape set to "dolphin", parameters set to 50 mm long, 25 mm wide, 18 mm high. Refer to the previous research to set the printing parameters[63]. The model was placed at room temperature for 1 h and photographed and recorded.

### Statistical analysis

All tests were repeated three times in parallel to obtain the average value. Data were processed using IBM SPSS Statistics 22 statistical software (IBM SPSS Inc., Chicago, USA). The significance of the experimental results was determined using ANOVA ($p < 0.05$). The experimental results were plotted using Origin 9.1 software from OriginLab Corp.

## Data availability

The authors declare that the data supporting the findings of this study are available within the paper. Any raw data files in another format are available from the corresponding author upon reasonable request.

Received: 15 October 2025; Accepted: 4 January 2026;
Published online: 13 January 2026

## References

1. Wen, J., Zhao, J., Jiang, L. & Sui, X. Oil-water interfacial behavior of zein–soy protein composite nanoparticles in high internal phase Pickering emulsion. *Food Hydrocoll.* **149**, 109659 (2024).
2. Zhao, Q., Fan, L., Li, J. & Zhong, S. Pickering emulsions stabilized by biopolymer-based nanoparticles or hybrid particles for the development of food packaging films: a review. *Food Hydrocoll.* **146**, 109185 (2024).
3. Yang, Z. et al. Pickering emulsions stabilized by soybean protein-based nanoparticles: a review of formulation, characterization, and food-grade applications. *Compr. Rev. Food Sci. Food Saf.* **24**, e70157 (2025).
4. Yue, Y., Jiang, Y. & Shi, J. The effects of ultrasonic pretreatment and enzymatic modification on the structure, functional properties, and in vitro digestion of whey protein isolate. *Foods* **14**, 1445 (2025).
5. Türker, D. A. Influence of charged polysaccharides and zein nanoparticles on the interfacial and emulsification properties of Pickering emulsions. *Food Hydrocoll.* **161**, 110887 (2025).
6. Jiang, R., Xu, Y. & Zhou, Z. Impact of interfacial rigidity on the rheological properties of high internal phase Pickering emulsions stabilized by casein, walnut protein isolate, and their complexes. *Food Hydrocoll.* **162**, 111030 (2025).
7. Kheto, A. et al. A review on advancements in emerging processing of whey protein: enhancing functional and nutritional properties for functional food applications. *Food Saf. Health* **3**, 23–45 (2025).
8. Chen, Y., Cai, Y., Di, Z., Zhao, M. & Zhao, Q. Improving quality characteristics of whipped cream based on novel additives: a review of current status, challenges, and strategies. *Food Bioprocess. Technol.* **18**, 55–81 (2025).
9. Han, Y. M., Zhu, L., Qi, X. G., Zhang, H. & Wu, G. C. Characteristics of low-fat whipped cream containing protein-based fat replacers. *Int. J. Dairy Technol.* **76**, 276–290 (2023).
10. Yu, X. et al. Preparation and 3D printing of high internal-phase Pickering emulsions stabilized by chicken egg white microgel. *Food Hydrocoll.* **147**, 109393 (2024).
11. Shahbazi, M., Jäger, H., Chen, J. & Ettelaie, R. Construction of 3D printed reduced-fat meat analogue by emulsion gels. Part II: printing performance, thermal, tribological, and dynamic sensory characterization of printed objects. *Food Hydrocoll.* **121**, 107054 (2021).
12. Sun, H. et al. Enhancement of the formation and stability of low-fat Pickering emulsion gels stabilized with egg yolk granules-chitosan complex: insights into the development of mayonnaise substitutes. *Food Chem.* **464**, 141734 (2025).
13. Larcinese-Hafner, V. & Erni, P. Tannin-on-protein adlayers: secondary adsorption quantified by quartz crystal microbalance with dissipation monitoring (QCM-D). *Food Hydrocoll.* **157**, 110443 (2024).
14. Han, X., Liang, Z., Tian, S., Liu, L. & Wang, S. Modification of whey −soybean mixed protein by sequential high-pressure homogenization and transglutaminase treatment. *LWT–Food Sci. Technol.* **172**, 114217 (2022).
15. Cui, Q. et al. Improving the gel properties of transgenic microbial transglutaminase cross-linked soybean–whey mixed protein by ultrasonic pretreatment. *Process Biochem.* **91**, 104–112 (2020).
16. Wu, C. et al. Interaction of alkyl gallate with gliadin and its effect on the surface and foaming properties of composite nanoparticles. *Food Hydrocoll.* **163**, 111096 (2025).
17. Ban, Q. et al. Effect of non-covalently bound alkaline amino acids on the structural characterization, microstructure, and rheological properties of whey protein emulsion gel. *LWT–Food Sci. Technol.* **209**, 116809 (2024).
18. Xie, H. et al. How the ovalbumin modulates the conformation of zein through protein–protein interactions. *Food Hydrocoll.* **159**, 110696 (2025).
19. Wang, S., Cui, Y., Sun, Y., Yu, G. & Wang, T. Insight into the effects of soybean isoflavone on the functional properties of rice bran protein: focus on non-covalent interaction. *LWT–Food Sci. Technol.* **217**, 117346 (2025).
20. Ma, N., Zhang, B., Yan, X. & Wang, X. Transglutaminase-assisted covalent modification of soybean protein isolates with γ-aminobutyric acid: effects on structure and gel properties. *Food Hydrocoll.* **164**, 111157 (2025).
21. Zhang, W. et al. Effect of ultrasound-assisted ionic liquid pretreatment on the structure and interfacial properties of soy protein isolate. *Process Biochem.* **115**, 160–168 (2022).
22. Jin, D. et al. A study on the synergistic interaction of pea protein isolate and whey protein isolate for enhancing the stability and quality of krill oil emulsion. *Food Hydrocoll.* **157**, 110426 (2024).
23. Rao, Y., Deng, J., Zhang, C., Song, Y. & Liu, L. Probiotics encapsulated by calcium pectin/chitosan–calcium pectin/sodium alginate–pectin–whey through biofilm-based microencapsulation strategy and their preventive effects on ulcerative colitis. *Food Hydrocoll.* **158**, 110501 (2025).
24. Liu, X. et al. Effects of extrusion technology on physicochemical properties and microstructure of rice starch added with soy protein isolate and whey protein isolate. *Foods* **13**, 764 (2024).

25. Liu, Z. et al. 3D printing of curcumin enriched Pickering emulsion gel stablized by pea protein–carrageenan complexes. *Food Hydrocol.l* **146**, 109170 (2024).
26. Chen, B. et al. Differentiating the effects of hydrophobic interaction and disulfide bond on the myofibrillar protein emulsion gels at the high temperature and the protein interfacial properties. *Food Chem.* **412**, 135472 (2023).
27. Wu, Y. et al. Emulsification properties and oil–water interface properties of L-lysine-assisted ultrasonic treatment in sea bass myofibrillar proteins: influenced by the conformation of interfacial proteins. *Food Hydrocoll.* **147**, 109405 (2024).
28. Hong, Z., Kong, Y., Chen, J., Guo, R. & Huang, Q. Collaborative stabilizing effect of trehalose and myofibrillar protein on high internal phase emulsions: improved freeze–thaw stability and 3D printability. *Food Chem.* **469**, 142564 (2025).
29. Zhao, J. et al. Adsorption mechanism of soy protein amyloid fibrils with different morphological structures at the interface of oil-in-water emulsion. *Food Hydrocoll.* **162**, 110899 (2025).
30. Yu, S., Peng, G. & Wu, D. Effect of surface acetylation of chitin nanocrystals on the preparation and viscoelasticity of sunflower seed oil-in-water Pickering emulsions. *Int. J. Biol. Macromol.* **254**, 127883 (2024).
31. Zou, Y. et al. Effect of ultrasound combined with plasma protein treatment on the structure, physicochemical and rheological properties of myofibrillar protein. *Ultrason. Sonochem.* **112**, 107151 (2025).
32. Li, H. et al. Effects of different ultrasound powers on the structure and stability of protein from sea cucumber gonad. *LWT–Food Sci. Technol.* **137**, 110403 (2021).
33. Carbone, C. et al. Interfacial dilational rheology of chitosan–silica nanocomposite films at the aqueous dispersion/air interface. *J. Mol. Liq.* **425**, 127273 (2025).
34. Tong, X. et al. Changes in structure, rheological property and antioxidant activity of soy protein isolate fibrils by ultrasound pretreatment and EGCG. *Food Hydrocoll.* **122**, 107084 (2022).
35. Huang, L., Jia, S., Zhang, W., Ma, L. & Ding, X. Aggregation and emulsifying properties of soybean protein isolate pretreated by combination of dual-frequency ultrasound and ionic liquids. *J. Mol. Liq.* **301**, 112394 (2020).
36. Gao, Y. et al. Ability of soy protein derived amyloid fibrils to stabilize aqueous two-phase system and effect of pH on the system. *Food Hydrocoll.* **145**, 109084 (2023).
37. Tian, Y. et al. Emulsifying properties of egg proteins: Influencing factors, modification techniques, and applications. *Compr. Rev. Food Sci. Food Saf.* **23**, e70004 (2024).
38. Cai, Z. et al. Correlation between interfacial layer properties and physical stability of food emulsions: current trends, challenges, strategies, and further perspectives. *Adv. Colloid Interface Sci.* **313**, 102863 (2023).
39. Ye, Z., Wang, J., Ma, G. & Ma, J. Ultrasound and glycosylation modifications enhance the physicochemical and functional properties of canola protein isolate for O/W emulsion stabilization. *Food Chem: X* **28**, 102535 (2025).
40. Zhang, X. et al. Effects of the interaction between bacterial cellulose and soy protein isolate on the oil–water interface on the digestion of the Pickering emulsions. *Food Hydrocoll.* **126**, 107480 (2022).
41. Wei, Y. et al. Interfacial and emulsion characterisation of chemically modified polysaccharides through a multiscale approach. *J. Colloid Interface Sci.* **580**, 480–492 (2020).
42. Yin, M., Hao, H., Wei, H., Li, M. & Shao, Z. In situ adsorption study of carboxymethylcellulose and sodium oleate on quartz using a quartz crystal microbalance with dissipation (QCM-D). *Colloids Surf. A* **685**, 133197 (2024).
43. Wang, L. et al. The rheological/interfacial behavior and stability properties of nanoemulsions prepared using whey protein–carboxymethyl chitosan conjugates. *Colloids Surf. A* **662**, 130924 (2023).
44. Tian, Y. et al. Interfacial properties of whey protein hydrolysates monitored by quartz crystal microbalance with dissipation. *Int. J. Biol. Macromol.* **301**, 140368 (2025).
45. Zhou, Q., Wang, W., Jiang, Z., Cao, Y. & Xiao, J. Enhancing stability of Pickering emulsions: insights into the interfacial dynamics of Zein–MCT composite nanoparticles. *Food Hydrocoll.* **148**, 109504 (2024).
46. Guo, Y. et al. Effect of heat treatment on the structural and emulsifying properties of copra meal protein: improving interfacial properties to enhance performance of its Pickering emulsion. *Food Chem.:X* **22**, 101442 (2024).
47. Yu, M. J., Feng, R., Long, S., Tao, H. & Zhang, B. Stabilizing emulsions by ultrasound-treated pea protein isolate-tannic acid complexes: impact of ultrasonic power and concentration of complexes on emulsion characteristics. *Food Chem.* **463**, 141266 (2025).
48. Zhang, J. et al. Application of soy protein isolate–naringenin complexes as fat replacers in low-fat cream: based on protein conformational changes, aggregation states and interfacial adsorption behavior. *Int. J. Biol. Macromol.* **274**, 133315 (2024).
49. Atik, I., Tekin Cakmak, Z. H., Avcı, E. & Karasu, S. The effect of cold press chia seed oil by-products on the rheological, microstructural, thermal, and sensory properties of low-fat ice cream. *Foods* **10**, 2302 (2021).
50. Li, J. et al. Consequence of high-pressure homogenization on the whipping characteristics of soybean oil body cream. *Food Chem.* **468**, 142450 (2025).
51. Chakraborty, S., Deka, G., Bora, J. & Dutta, H. Debittered pomelo (*Citrus maxima*) seed powder as a functional ingredient in low-fat ice cream. *Sustain. Food Technol.* **3**, 2009–2031 (2025).
52. Xia, C. et al. The stabilization mechanism of the pea protein and rutin complex at the gas/liquid interface and its application in low-fat cream. *Food Chem.: X* **25**, 102140 (2025).
53. Yan, G. et al. Multiscale approach to the characterization of the interfacial properties of micellar casein and whey protein blends and their effects on recombined dairy creams. *Food Res. Int.* **188**, 114453 (2024).
54. Qian, S. et al. Low-fat-high-stability non-dairy whipping cream prepared from soybean oil bodies as a substitute for hydrogenated oil: impact of substitution ratio on structural properties, foam properties and sensory evaluation. *Food Chem.: X* **31**, 103077 (2025).
55. Ma, Z. et al. Effects of combined enzymatic and ultrasonic treatments on the structure and gel properties of soybean protein isolate. *LWT–Food Sci. Technol.* **158**, 113123 (2022).
56. Wang, N., Wang, X., Zhang, S., Wang, T. & Yu, D. Non-covalent interaction between soybean protein isolate and naringenin: focused on binding mechanism, interface behavior, and functional properties. *Food Hydrocoll.* **153**, 109975 (2024).
57. Jia, Y. et al. Different interactions driving the binding of soy proteins (7S/11S) and flavonoids (quercetin/rutin): alterations in the conformational and functional properties of soy proteins. *Food Chem.* **396**, 133685 (2022).
58. Sun, Y. et al. Co-microencapsulation of *Lactobacillus paracasei* and *Inonotus obliquus* polysaccharide in alginate system: physicochemical and functional properties. *Food Hydrocoll.* **166**, 111344 (2025).
59. Li, L. et al. Fabrication of water-in-oil-in-gel emulsion gel based on pH-shifting soybean lipophilic protein and carboxymethyl chitosan: gel performance, physicochemical properties and digestive characteristics. *Food Hydrocoll.* **147**, 109385 (2024).
60. Zhao, H., Xu, X., Yuan, B., Qi, B. & Li, Y. Fibrillation of soy protein isolate in the presence of metal ions: structure and gelation behavior. *Food Chem.* **453**, 139672 (2024).

61. Arrieira, N. M. et al. Oleogels based on carotenoid-rich microbial oil produced by *R. mucilaginosa* in agro-industrial by-products. *Bioprocess Biosyst. Eng.* **48**, 275–286 (2024).
62. Hou, J. et al. High internal phase Pickering emulsions stabilized by egg yolk–carboxymethyl cellulose as an age-friendly dysphagia food: tracking the dynamic transition from co-solubility to coacervates. *Carbohydr. Polym.* **342**, 122430 (2024).
63. Li, H. et al. Walnut protein-based 3D printed cream substitute. *J. Food Eng.* **357**, 111607 (2023).

## Acknowledgements

This work was financially supported by Key Research and Development Program of Heilongjiang (2024ZX10B10).

## Author contributions

Y. Sun wrote the main manuscript text and prepared all figures. Y. Sun and W. Guo did the formal analysis. X. Li did the investigation and data curation. L. Guo provided guidance on the methodology. L. Guo and Y. Jiang proposed the idea and supervision. L. Guo and Y. Zhang supported the funding acquisition. All authors reviewed the manuscript.

## Competing interests

The authors declare no competing interests.

## Additional information

**Supplementary information** The online version contains supplementary material available at https://doi.org/10.1038/s41538-026-00710-0.

**Correspondence** and requests for materials should be addressed to Yu Zhang.